

FLUID DYNAMIC MODEL OF THE MOLTEN SALT REACTOR EXPERIMENT

FLUID DYNAMIC MODEL OF THE MOLTEN SALT REACTOR EXPERIMENT USING
FLOWNEX SIMULATION ENVIRONMENT

By SEAN CRAWFORD, B.A.Sc.

A Thesis Submitted to the School of Graduate Studies in Partial Fulfilment of the Requirements
for the Degree Master of Applied Science

McMaster University © Copyright by Sean Crawford, December 2023

McMaster University MASTER OF APPLIED SCIENCE (2023) Hamilton, Ontario

TITLE: Fluid Dynamic Model Of The Molten Salt Reactor Experiment Using Flownex Simulation Environment

AUTHOR: Sean Crawford, B.A.Sc

SUPERVISOR: Professor D. Novog

NUMBER OF PAGES: xi, 62

Lay Abstract

Molten Salt Reactors (MSRs) are a next-generation nuclear reactor type desirable for improved safety, cost, and performance. This thesis seeks to analyze the Molten Salt Reactor Experiment (MSRE), the only MSR to have operated, to create inputs for a model that can be used to simulate the MSRE. This is done to prove the reliability of computer codes in simulating MSRs and support modelling approaches for future MSRs. A computer model of the system fluid dynamics was developed from these inputs in Flownex Simulation Environment, a computer software being used to develop new nuclear reactor designs. This Flownex model was compared against MSRE experimental data and found to be in good agreement, allowing future work to use these inputs and model to create a full model of the MSRE for analysis.

Abstract

Molten salt reactors (MSRs) have recently experienced renewed interest due to their potential for improved economics, safety, and sustainability. Despite their 70-year history, the Molten Salt Reactor Experiment (MSRE) was the only MSR to ever be operated and has become an essential source of experimental data for new MSR designs. This work evaluates available literature on the MSRE to create a model that serves as the basis for a thermalhydraulic analysis of the system.

It was proposed to create a model of the MSRE hydraulic experiment with geometric and head loss inputs calculated from first principles and accepted experimental results, as existing thermalhydraulic models tune inputs to match pressure loss and velocity data. Such a model is essential for modelling transient behaviour of the MSRE by ensuring that correct residence and neutron transport times are used for calculations. Minor head losses of components were calculated using accepted literature for similar geometries, and major losses were modified in the core to account for developing flow conditions and the atypical channel geometry.

Flownex Simulation Environment is a 1-dimensional software code that provides the ability to model entire nuclear reactor systems. A Flownex network of the MSRE was created to compare results against available MSRE experiment results, and results from the model agreed well in most cases. Pressure loss through the core and the full system were within 2% of experimental values. Velocities and flow rates matched well, except in regions of complex 3-dimensional flow such as the cooling annulus.

The model can easily be extended to simulate the full MSRE operating with molten salt, though no experimental data is available for comparison. Further investigation is required to ensure that correct heat transfer correlations and material properties are used. Flownex also has the potential to include neutronics in future simulations, allowing for the simulation of transient studies that were conducted with the MSRE.

Acknowledgements

Firstly, I would like to express my gratitude to my supervisor, Professor David Novog, who provided great support and allowed me the freedom to pursue a research topic of particular interest to me. Without his assistance I would not have had the opportunity and success in the nuclear engineering field that I have today.

Secondly, I want to thank my friends and family for their support over the last few years while I returned to school. I especially want to thank my partner Michaela Scanlon for her continuous patience, love, and time as I finished writing this thesis.

Finally I would like to thank those that helped me along the way with this research; the thermalhydraulics team at Terrestrial Energy and the Flownex support team both made the modelling, improving, and technical problem solving of this research project go much more smoothly. I would also like to thank Dr. Alex Rashkovan for his recommendations in accounting for non-circular channel major losses, as he saved me a great deal of time.

Contents

1. Introduction.....	1
2. Literature Review	3
2.1. General Molten Salt Reactors.....	3
2.2. Liquid-Fuel Molten Salt Reactors	4
2.3. Molten Salts and MSR Development Activities	5
3. The Molten Salt Reactor Experiment (MSRE).....	7
3.1. Equivalent Hydraulic Experiment.....	10
3.2. Data Discrepancies and the 5-Region Model.....	11
3.3. MSRE Design and Measurements.....	12
3.3.1 Volute (Distributor) and Cooling Annulus.....	13
3.3.2 Lower Head	16
3.3.3 Graphite Lattice Support Grid	18
3.3.4 Core.....	19
3.3.5 Upper Head and Outlet.....	22
3.3.6 Upper Plenum Short Circuit	23
3.4. Thickening Agent Studies	24
4. Flownex Simulation Environment Model	25
4.1. Flownex Model Simplifications	25
4.2. Model Input Data	26
4.2.1 Minor Losses	28
4.2.2 Core Channel Major Loss.....	31
4.2.3 Hydraulic Model Material Data.....	34
4.3. Flownex Hydraulic Model	34
4.3.1 Reactor Geometry Chart (RGC).....	34
4.3.2 Additional Model Components	40
5. Hydraulic Model Results Comparison.....	41
5.1. Similar Studies of the MSRE	41
5.2. Flownex Model vs Experimental Results.....	41
5.3. Sensitivity Studies	44
5.3.1 Upper Plenum Short Circuit Inclusion	44

5.3.2 Graphite Core and Grid	45
5.3.3 Other Model Components.....	47
5.3.4 Summary.....	50
6. Conclusions	51
6.1. Recommendations for Future Work.....	52
7. References.....	54
Appendix A – Summary of Flownex Model Inputs.....	59
Appendix B – Summary of Discrepancies in Previous Work and Reported Values	61

Table of Figures

Figure 1: Cutaway View of the Molten Salt Reactor Experiment Core [42].....	8
Figure 2: Cross Section of MSRE Core [16, p. 76]	9
Figure 3: Assembled Half-Section of MSRE Graphite Core and Lattice [43]	10
Figure 4: Assembled Equivalent Hydraulic Experiment [44].....	11
Figure 5: Head Loss from 5" Inlet to 5" Outlet Pipe [37].....	13
Figure 6: Inlet Distributor and Distributor Orifices Flow Path.....	13
Figure 7: Elevation of MSRE and Select Internal Components	14
Figure 8: Cooling Annulus Flow Path	15
Figure 9: Volute Centerline Velocity as a Function of Angle [37].....	15
Figure 10: Annulus Centerline velocity along the Annulus Length [37].....	16
Figure 11: Assembly of Anti-Swirl Vanes and Drain Line in the Lower Head [42].....	16
Figure 12: Image from the INOR-8 Support Grid and Dowels in the Lower Plenum [47]. The main image is before MSRE operation, and the bottom right image is after operation.	17
Figure 13: Lower Head Radial Pressure Gradient [37]	18
Figure 14: Experimental Head Loss through the Graphite Support Grid and Core [37] ...	19
Figure 15: Graphite Core Stringer Geometry and Channel Dimensions [16].....	20
Figure 16: Control Rod and Sample Basket in Core [16].....	20
Figure 17: Experimental Core Channel Flow Rates [37].....	21
Figure 18: Upper Head and Outlet Geometry [40]	22
Figure 19: Upper Head Experimental Velocity Profile [37].....	23
Figure 20: Reactor Vessel Lugs above Volute Orifices [51]	24
Figure 21: Bottom view of the central region of core and graphite grid. Light grey lines (not passing through dowels) represent the INOR-8 support structure [54].....	27
Figure 22: Inlet, Volute (Distributor), and Orifices of the MSR (Left) and Flownex Network (Right)	28
Figure 23: Zoom-in of Anti-Swirl Vane Region.....	29
Figure 24: Zoomed-in MSRE Regions: Core-Can Gap (Left), Fuel Short Circuit (Middle), and Outlet Tee (Right)	31
Figure 25: Scaled Experimental Data Estimating Entrance Length Friction Factors	33
Figure 26: Colour-Coded Cross Section of the MSRE Core Indicating RGC Zones	36
Figure 27: Flownex Reactor Geometry Chart for the MSRE Hydraulic Experiment.....	37
Figure 28: Zoomed Geometry of Flownex Network	38
Figure 29: Flownex Network Model of the MSRE Hydraulic Experiment.....	39

List of Tables

Table 1: Model Input Parameters Summary	26
Table 2: Hydraulic Model Core Input Geometry Parameters for Flownex Reactor Geometry Chart.....	27
Table 3: Flownex vs Experimental Results - Residence Time [16, p. 102].....	42
Table 4: Flownex vs Experimental Results - Mass Flow	42
Table 5: Flownex vs Experimental Results - Velocity	43
Table 6: Flownex vs Experimental Results - Pressure Loss	43
Table 7: Flow Rate and Velocity for Core including Fuel Short Circuit.....	44
Table 8: Sensitivity Study of the Graphite Grid on Flow Parameters	45
Table 9: Sensitivity Study Results of Core Parameters	47
Table 10: Summary of Sensitivity Studies of Model Inputs.....	50
Table 11: Complete Flownex Model Inputs	59
Table 12: Complete Reactor Geometry Chart Inputs for the Hydraulic Experiment	60
Table 13: Summary of Major Discrepancies Observed in Key Hydraulic Model Values.	61
Table 14: Comparison of Select MSRE Models in Literature	62

List of Abbreviations and Symbols

AOO	Anticipated Operational Occurrences
ARE	Aircraft Reactor Experiment
BWR	Boiling Water Reactor
CAD	Computer Aided Design
CFD	Computational Fluid Dynamics
DBA	Design Basis Accident
MSR	Molten Salt Reactor
MSRE	Molten Salt Reactor Experiment
ORNL	Oak Ridge National Laboratory
PWR	Pressurized Water Reactor
PHWR	Pressurized Heavy Water Reactor
RGC	Reactor Geometry Chart
	
A	Area
D_h	Hydraulic Diameter
f	Friction Factor
K	Loss Coefficient
L	Length
P	Pressure
Q	Flow Rate
Re	Reynold's Number
v	Velocity
ρ	Density

Declaration of Academic Achievement

The author hereby declares that all research, analysis, figures, results, computer code, and other items contained within this thesis are the work of the author, other than those referenced, as the sole contributor to this thesis.

1. Introduction

As global climate change issues become more prevalent worldwide, efforts to reduce fossil fuel usage for energy production is paralleled by increasing energy demands. Renewable energy currently accounts for less than 30% of global power production and needs to reach almost 60% by 2030 to remain on track with worldwide pledges for fossil fuel reductions [1]. This level of increase faces substantial challenges, and nuclear power offers a promising solution. The technology and expertise exists today for nuclear power to provide a sustainable and reliable green energy baseload to meet global greenhouse gas emission targets.

The demand for nuclear power is immediate, with 45 GW of production slated to be retired and only 64 GW of planned additions by 2050 [2]. Unfortunately, nuclear power has faced significant criticism and poor public perception in the wake of the Chernobyl and Fukushima disasters; more than three times the number of reactors were constructed in the 20 years prior to the event than the 20 years following the Chernobyl accident [3]. 94% of reactors operating today are of the boiling water (BWR), pressurized water (PWR) or pressurized heavy water reactor (PHWR) type. New reactor designs seek to improve the build and operating cost, flexibility in fuel type, and – most importantly to the public perception of nuclear energy – safety. Many new types of reactors have been proposed and researched since the advent of the water reactor technology. Molten Salt Reactors (MSRs) have become a topic of intense interest in recent years after being selected as one of six Generation IV reactor types by the Generation IV International Forum, though the design has existed for over 70 years [4].

In order to prove the safety of reactor designs, stringent regulations and standards are in place such as CNSC REGDOC 2.4.1 and 2.5.2. The rigor of proving the operability and safety of reactor designs is part of the attraction of continuing to build proven reactor types. Simulations have become essential to all areas of engineering, and modern computer codes allow the assessment of innovative designs on a scale much greater than was possible for the first generation of nuclear reactors. Attention has turned to comprehensive computer simulations rather than expensive experiments for proving the behaviour and response of new reactor designs.

Two inter-related concepts provide the foundation for analyzing nuclear reactor design: neutronics, the study of neutron conservation in sustaining the fission chain reaction in the fuel; and thermalhydraulics, the study of heat production and transport in the system by a fluid. The coupling of these two concepts drives the study of reactor designs to comply with regulations during normal operation, as well as proving their safety for Anticipated Operational Occurrences (AOOs) and Design Basis Accidents (DBAs).

There are many existing tools to simulate reactor thermalhydraulics, from component level Computational Fluid Dynamics (CFD) codes to system level codes such as RELAP5, TRACE, and GOTHIC. Many of these codes provide either internal neutronics or coupling to neutronics software, though many also have specific use cases and limitations. This work seeks to create a thermalhydraulic model of a molten salt reactor and compare it to experimental data using one such system level code, Flownex Simulation Environment. This model, built from fundamental

first principles and accepted experimental data, will be used to perform the reference and sensitivity studies for an important molten salt reactor experiment.

Beyond safety considerations, many other difficulties face new reactor designs. New supply chains must be established for reactor components, and in many cases, nuclear fuel. Challenges such as identifying new materials for properties like corrosion resistance or for high temperature operation are often faced by next generation reactor designs.

2. Literature Review

This section describes the design features of various Molten Salt Reactors (MSRs), as there are many types of designs. It will also briefly discuss research in areas that are integral to MSR operations, such as molten salt properties.

2.1. General Molten Salt Reactors

The key design feature of molten salt reactors is the use of molten salt as a heat transport system coolant. While there are many types of molten salts, fluoride-based salts are the most popular and are already used today in the aluminum and uranium industries due to having a single stable isotope [4]. In general, molten salts are stable compounds with melting points of a few hundred degrees Celsius and boiling points well over a thousand Celsius, with heat retention capabilities that make them ideal for thermal storage or high temperature heat transport systems [5]. The attraction of MSRs has centered around two key points: the potential to use a variety of fuels, and their inherent safety.

Many concepts of MSRs have been proposed. While they can be operated with solid fuel with a molten salt coolant, the focus of this thesis is on fuel mixed with the molten salt, which provides a variety of benefits not available to other reactor types. This section describes general MSR design with a molten salt coolant, with the following section discussing the benefits and challenges of fuel mixed directly with the coolant salt.

The technological benefits of MSRs are numerous. Their high operating temperatures greatly improve efficiency, and also allow for industrial heat applications in the cement, steel, oil and chemical industries [6]. MSRs can also be refuelled while remaining online; while this feature is shared by a number of Generation IV reactors, few existing reactor designs have this feature. Another major benefit of MSRs is their ability to operate with different fuels, such as uranium, plutonium, actinide fluoride, or thorium [4]. This allows them to function as standard power reactors, nuclear waste burners, or breeder reactors. The ability to run on the thorium fuel cycle is of high interest as thorium is three to four times more abundant in the Earth's crust than uranium [7] [8]. The thorium fuel chain requires substantially less fuel material and produces several orders of magnitude less transuranic waste than conventional uranium-based reactors [8]. Thorium is more easily extracted from the Earth's crust and is often a byproduct of rare earth metal mining [8] [9]. Thorium has additional benefits regarding proliferation resistance. ^{232}U is produced alongside ^{233}U and is a strong gamma emitter with a short half-life [8]. These gammas are both easily detectable and destructive. Furthermore, ^{232}U is inseparable from ^{233}U . While alternative fuels can be used in MSRs in traditional solid fuel form, a number of benefits stem from dissolving the fuel in the coolant salt; this is discussed in the following section.

Safety is a primary concern for all Generation IV reactors, especially from the perspective of the general public. Molten salt reactors exhibit a number of inherent safety characteristics. Prominently, MSRs contain no liquid water and operate at near atmospheric pressure, meaning a steam explosion - like occurred in the Chernobyl accident - is impossible [6]. The high boiling point of molten salts makes evaporation impossible, meaning the pressure within the system cannot increase. Additionally, the absence of water and zirconium alloys prevents the possibility of a hydrogen explosion like occurred at Fukushima-Daiichi.

Finally, a station blackout is a critical scenario where the reactor experiences a total loss of power, both from off-site and emergency back-up sources [10]. In such an event, molten salt reactors may use natural circulation of the coolant salt, rather than forced convection, through a static air cooler to still allow the minimum amount of decay heat to be removed from the system [6].

Despite these excellent traits, a number of design barriers are part of the reason behind the lack of molten salt reactors in operation today. There is a large variety of molten salts, and due to this, only the material properties of a few of the most popular salts are known to the required degree of accuracy. There are known issues with molten salts such as their corrosivity, which makes material selection challenging for nuclear applications, especially at high temperature [4]. The main material developed for structural components in MSR is Hastelloy N, which is only rated to 704°C [7].

2.2. Liquid-Fuel Molten Salt Reactors

This section describes MSR with the fuel dissolved in the molten salt coolant. These MSR have all of the features described in the general MSR section above, plus a handful of other benefits and challenges.

One of the biggest advantages is unique to liquid fuel. Online fuel reprocessing allows the removal of gaseous fission products like xenon and krypton as they bubble out of the liquid, while other transuranic elements are salt soluble and remain in the core until destroyed [4]. This offers greatly improved fuel burn-up, as solid uranium fuel rods are typically removed after about 4% of their potential energy is used due to poison build-up inside the solid fuel elements reducing the neutrons available to sustain the reaction [8].

Solid fuel is also subject to stresses from internal temperature gradients and fission product accumulation, and the cladding becomes damaged over time due to the radiation. Most current reactor designs require shut down approximately every 18 months to replace or rearrange fuel rods with structural damage. As this is not an issue with liquid fuel, there are substantial savings due to eliminating fuel element fabrication and reducing reactor shutdowns.

A prominent design safety feature of liquid fuel MSR is the ability to drain the reactor to a holding tank, completely stopping the fission reaction. A commonly proposed method for this is using a frozen fuel salt plug; with a loss of power, operator intervention, or large temperature increase in the salt, the fuel salt plug warms up and melts to automatically drain the core [6]. Low pressure operation also reduces the risk of piping ruptures, with a breach causing a leak rather than an explosion. Salt will drip from the leak and solidify after cooling.

These reactors are also self-regulating due to the salt expanding as it heats up, leading to a negative void and temperature reactivity coefficient [7]. This thermal expansion reduces the reactivity and causes temperature to fall [8]. Removing more heat from the core for increased power generation causes the temperature to rise due to increased fission in the core. This allows for passive load following, as no operator intervention is required to respond to changing electricity demands, making MSR ideal for coupling with inconsistent renewable energies like

wind and solar. Load following also benefits from the removal of the gaseous fission poisons like xenon, as described above.

Liquid fuel is also highly beneficial for non-proliferation of nuclear material, as the dissolved fuel cannot be easily separated, and the fabrication and transport of new fuel elements is avoided [4].

Importantly, all of the features outlined here, and in the section above on general molten salt reactors, are passive or inherent to the design of MSR. This is exceptionally desirable in modern reactor designs as it greatly improves reactor safety during operation and also provides a 'walk away safe' feature - meaning that for accident prevention they operate on passive safety systems indefinitely without operator intervention [11].

2.3. Molten Salts and MSR Development Activities

Research into MSRs began with the Aircraft Reactor Experiment (ARE) back in the 1940s and was followed shortly after by the only full-scale molten salt reactor to ever operate: the Molten Salt Reactor Experiment (MSRE) at Oak Ridge National Laboratory (ORNL) [7]. Despite this long history, the large variety in MSR uses and fuel types - as well as the lack of experimental results - has made progress on molten salt reactor design slow. A recent resurgence in interest in MSRs has led to mostly private companies leading research activities, and thus are not releasing most of their information on design activities.

As interest in MSRs increased, other uses of molten salts as coolants or heat transfer mediums gained traction. Substantial research is now available on various molten salts and their properties [12] [13] [14] [15] [16]. Two of the most popular salts historically are LiF-BeF₂ and LiF-NaF-KF, referred to as FLiBe and FLiNaK respectively. These salts are well studied and provide a good reference for desirable molten salt properties; while LiF alone melts at 500°C and boils at 1200°C, FLiNaK melts at 454°C and boils at 1570°C [17]. FLiBe melts at 459°C and boils at 1430°C. As salts exhibit different traits than their constituents, detailed studies are required for each new salt developed. FLiBe was used as the secondary salt in the Molten Salt Reactor Experiment, while the fuel salt was a mixture of UF₄, FLiBe, and ZrF₄, which was added to prevent the precipitation of UO₂ in the case of contamination [16].

Experimental measurements of various molten salts for their performance under different conditions has also been extensively studied. Fundamental studies such as laminar-turbulent transition regimes and heat transfer have substantial research available [18] [19] [20] [21] [22] [23] [24] [25] [26] [27]. Recently, heat transfer within heat exchangers has been a focus of experimental studies [28] [29] [30] [31]. These results are essential for MSR development, as widely used heat transfer correlations are not accurate for internally heated molten salts [32].

Research and development activities are occurring in a dozen countries worldwide on molten salts and MSRs [33]. Additionally, a large number of MSRs are currently under design in a number of countries, ranging from solid and liquid fuel concepts, thorium and uranium-based fuels, and thermal and fast spectrum designs [34]. Some are designed as standard power reactors, while others are designed as fuel breeders or waste burners. Other than the two experimental molten salt reactors operated at ORNL, only one MSR has been constructed. The Thorium-based

Molten Salt Experimental Reactor, or TMSR, was constructed at the Shanghai Institute of Applied Physics in China was reportedly completed in 2021 [35]. This 2 MWt test reactor, dubbed the TMSR-LF1, is a prototype for their planned 400 MWt reactor, the smTMSR-400; while the test reactor obtained an operating license in mid-2023, no further information on whether or not the reactor is operating was found at the time of writing [34] [36].

3. The Molten Salt Reactor Experiment (MSRE)

The Molten Salt Reactor Experiment (MSRE) was a graphite moderated reactor that used molten salt with dissolved fuel, and to date is the only full-scale MSR to ever be built and operated. The MSRE reactor was started in 1965 and ran until 1969 and operated on both ^{235}U and ^{233}U , though it never contained thorium [4]. As this reactor is the only source of experimental data for a fully operational molten salt reactor, it has been studied and simulated extensively; however, lack of operational data and missing or conflicting design reports has led to challenges using this data for designing new MSRs. Additionally, the MSRE was only built as a proof of concept and was never designed to run as a power reactor [16].

The MSRE was designed to operate at 10 MW thermal power, though it only ran at 7.3 MW [37] [38] [39]. The temperature increased from 1175°F (635°C) at the inlet to 1225°F (663°C) at the outlet after passing through 1140 channels machined in the graphite core [37]. The core was made up of 2 inch (50.8 mm) square stringers, with grooves machined into the faces to form channels for the molten salt fuel. A diagram of the reactor is shown in Figure 1, while a cross section of the reactor design is shown in Figure 2. An image of the actual core during assembly is shown below in Figure 3. The fuel salt used was $\text{LiF-BeF}_2\text{-ZrF}_4\text{-UF}_4$; the majority of operation and tests used enriched $^{235}\text{UF}_4$, which was eventually replaced with $^{233}\text{UF}_4$. While early reports on fuel composition indicate the thorium fuel chain was directly planned to be used, later project timelines indicate only ^{233}U was used with small additions of plutonium or uranium to sustain the reaction [16] [40] [41]. The majority of internal components made up from Hastelloy N (also known as INOR-8), a material developed specifically for the MSRE at Oak Ridge National Laboratory.

Unfortunately, due to the limited instrumentation available at the time of operation, almost no thermalhydraulic data of the MSRE could be taken during operation [37]. Two scale experiments were built to obtain flow information based on the MSRE geometry, as detailed in Section 3.3. While an abundance of studies have been done on the neutronics of the MSRE, both by ORNL at the time of operation and in recent years, the hydraulic experiments are the only source of thermalhydraulic information and must be carefully evaluated. Additionally, all software simulations of the MSRE that are available in literature either tune the model inputs to match the available experimental results, or do not provide the exact inputs used for modelling the reactor. Thus, a strong effort was made to create a thermalhydraulic model from fundamental geometry and loss calculations.

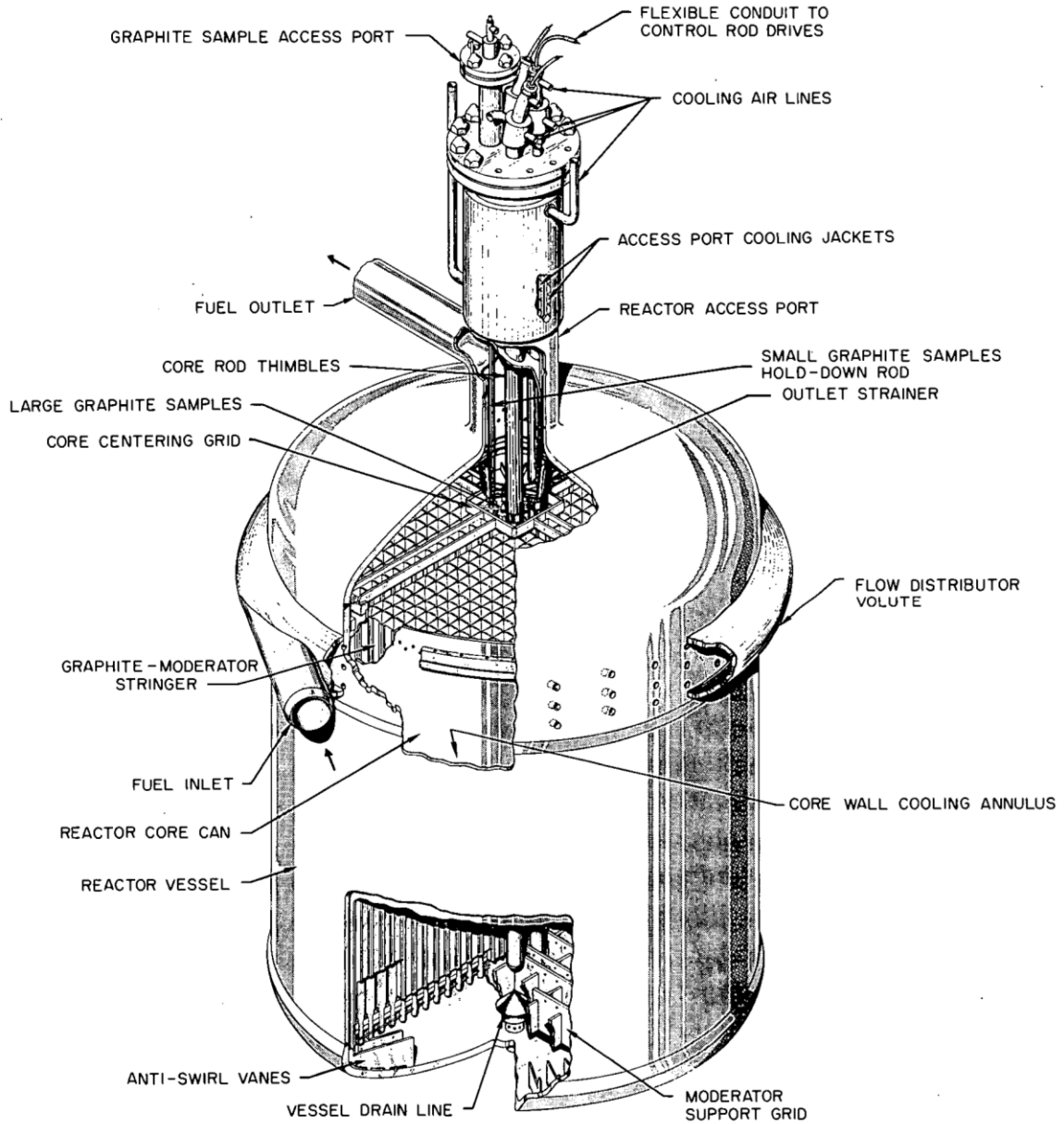


Figure 1: Cutaway View of the Molten Salt Reactor Experiment Core [42]

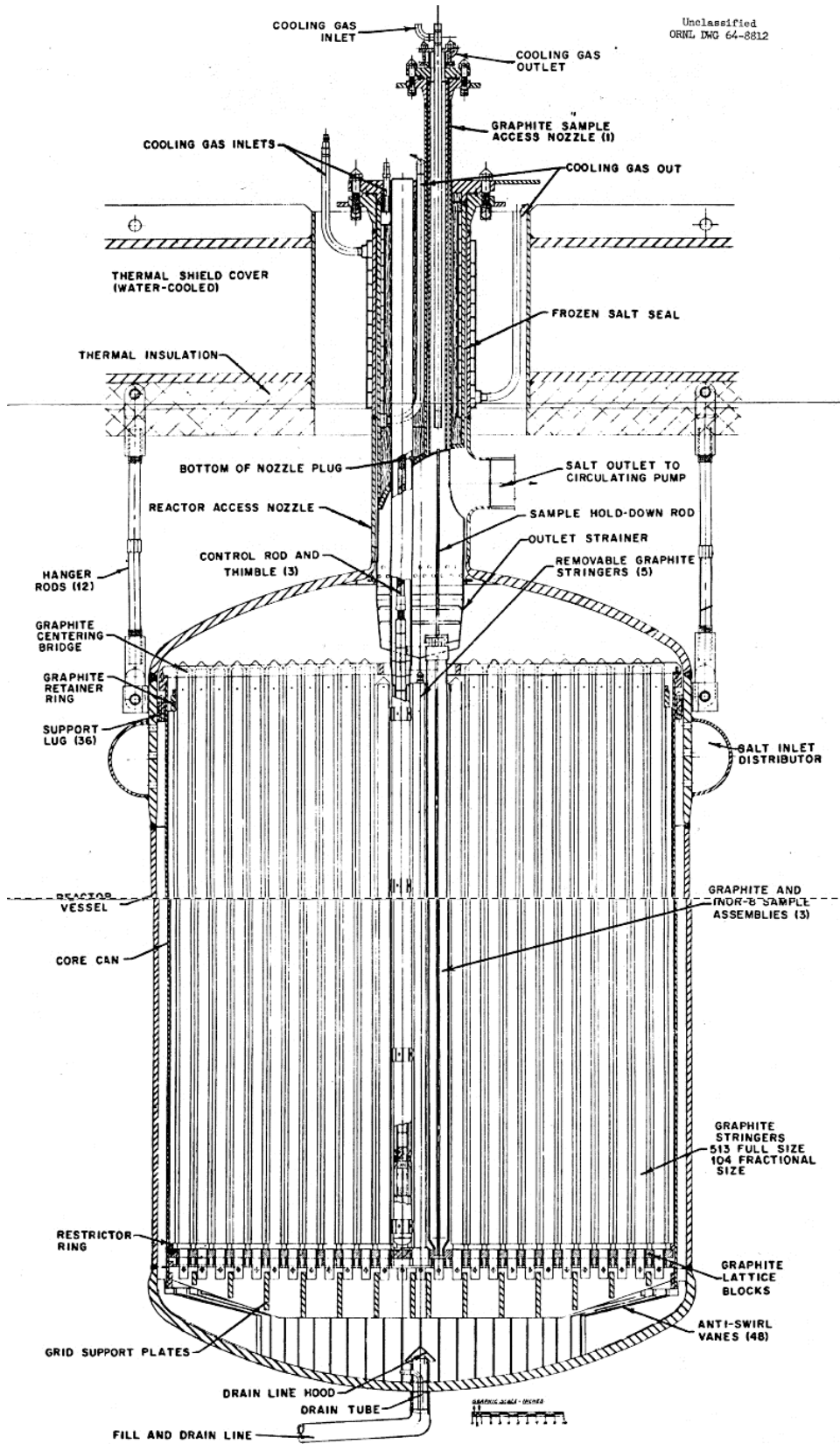


Figure 2: Cross Section of MSRE Core [16, p. 76]

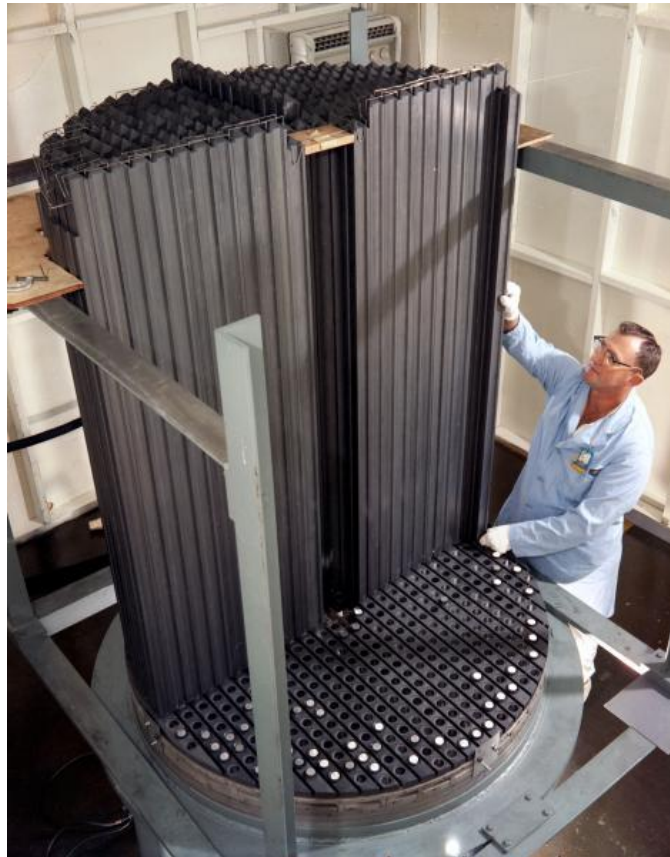


Figure 3: Assembled Half-Section of MSRE Graphite Core and Lattice [43]

3.1. Equivalent Hydraulic Experiment

Two hydraulic experiments of the MSRE were built and operated; the first was 1/5 scale which was primarily used as a proof of concept, so not many details are available. The second was a full-scale 1:1 scale experiment of the MSRE, shown in Figure 4, which provided many measurements of pressure losses and flow rates. These results are reported in their relevant description sections. The experiment was an exact replica of the MSRE, barring a few changes that are noted below [37]:

- The entire hydraulic experiment was constructed from carbon steel, except the graphite stringers and graphite grid, which were fabricated from aluminum.
- The dimensional tolerances of the experiment were normally double that of the MSRE, except where noted.
- The flow rate was tested for 300-1200 gallons/minute, but many of the reported experimental results were only for the high flow data. Only results for 1200 gallons/minute were studied in this report, as this effects head loss calculations.
- Additional windows and measurement apparatus were installed in the experiment and assumed to have no effect on the flow.

- The experiment was operated with water at 75-80°F, resulting in a Reynold's number approximately 4x that of the MSRE. A thickening agent to match the Reynold's number of the MSRE was added to confirm the results for some tests, discussed below.
- Certain geometric aspects were not included in the hydraulic experiment, such as the absence of the control rods and specimen holder in the core. These are mentioned in their respective sections.



Figure 4: Assembled Equivalent Hydraulic Experiment [44]

To avoid confusion, within this document 'MSRE' will refer to the final as-built Molten Salt Reactor Experiment that operated at full power and temperature, while the term 'hydraulic experiment' will be used to discuss the 1:1 scale experiment operated with water as the fluid and reported on by Kedl.

3.2. Data Discrepancies and the 5-Region Model

The majority of the geometry details for the MSRE came from the hydraulic experiment [37] and an MSRE Design and Operation report [16]. There are many instances of conflicting values for both geometry and hydraulic results, which are challenging to confirm as many reference documents and drawings for the MSRE were either never released publicly or lost over time. As many of the reports were released while the design and fabrication were ongoing, it is likely that some reported values were changed as the design proceeded. Major reports were based on the semi-annual progress reports published by ORNL, though many other minor or internal reports that are cited are not available. For the purposes of this study, the hydraulic experiment report by Kedl [37] was taken as the most accurate, as it was the most recently published. It is known that the hydraulic experiment studies were still ongoing at the time of the report by Robertson, as it is

noted that the results excluded modifications made to the graphite grid which are included in the report by Kedl [16, p. 100].

Any major discrepancies will be reported in the following sections and referenced; a summary of found discrepancies that impacted the creation of a hydraulic model is available in Appendix B – Summary of Discrepancies in Previous Work and Reported Values. One such major issue comes from the reported 5-region hydraulic model reported by Engel and Haubenreich [45]. The report references a design with 1064 channels; it was confirmed in [46] that there was another design of the MSRE that had 1064 channels and widely different geometry for the inlet volute, anti-swirl vanes, INOR-8 support structure, and core stringers, though exact geometric information was not found. The 5-region model attempted to modify the original hydraulic calculations to fit an 1140 channel core design; it was found that some regions in this model had values that differed significantly from expected results, such as fluid velocities in the outer 2" of the core of more than double that of the bulk [45]. The reason for this was not explained in the report and could not be reconciled with any other available information. Thus, it was assumed that it was based on an alternative MSRE design, and only values for the channel number per region and fuel fraction were used.

Another item of note is the referencing of the material INOR-8 – while this was the original name for the material developed for the reactor, it was changed to Hastelloy N at some point during the development and is still in use today under this name [4] [41, p. 2]. This is also cross-checked by comparing the chemical compositions reported for individual components, such as the control rod thimbles or support grid, that were listed as INOR-8 in older documents and Hastelloy N in newer documents [16] [47, p. 147] [48]. Throughout most of this document INOR-8 will be used, to remain consistent with the terminology in the references.

3.3. MSRE Design and Measurements

The following section describes the as-built geometry of the MSRE, as well as any changes made to the geometry for the hydraulic experiment that operated with water. Any measurements taken in the hydraulic experiment are also reported by region. The region of interest in this model starts at the 5" fuel inlet pipe just before the flow distributor and ends at the 5" fuel outlet pipe at the outlet of the tee on top of the MSRE can. As such, no attempt to model the additional piping, pumps, heat exchangers, or additional systems from first principles was made. The geometry of the MSRE can be clearly seen in the cutaway drawing in Figure 1 and the cross-section drawing in Figure 2.

All reported values were in imperial units. As such, it is often more convenient to refer to values in their reported values, such as pipe diameters in inches and flow rates in gallons/minute. All values except flow rates have been converted to SI units in Section 5.

The pressure loss through the entire MSRE from 5" inlet pipe to 5" outlet pipe was measured in the hydraulic experiment and is shown below in Figure 5. It is noted that the value from this graph for 1200 gallons/minute, approximately 15 ft-fluid, directly conflicts with the graph and reported value by Robertson of 9.2 ft-fluid [16, p. 91].

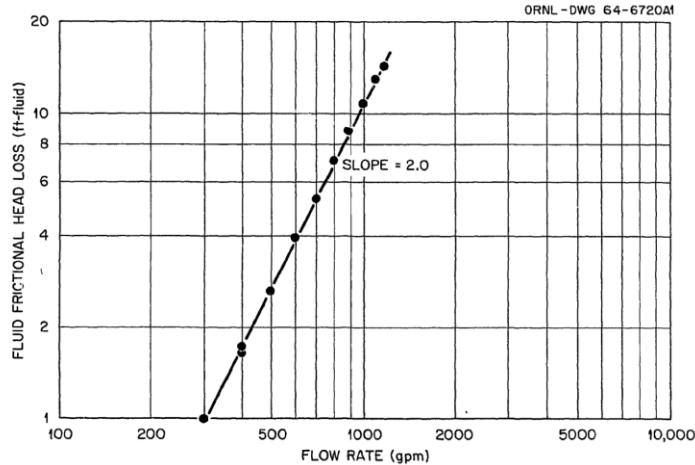


Figure 5: Head Loss from 5" Inlet to 5" Outlet Pipe [37]

3.3.1 Volute (Distributor) and Cooling Annulus

The loop piping is a standard 5" schedule 40 pipe, which expands to 6" schedule 40 before entering volute [37]. From Figure 4, it appears the distance from the volute inlet to the pressure sensor in the hydraulic experiment is approximately 22" in length. The pipe expansion was added to closely match the cross-sectional area of the volute. The volute is a semi-circular design that wraps the reactor vessel, with the tail connecting to the head to provide recirculation. The inner radius of the volute is 4.07", as calculated from the provided area of 26 in² [37] [16]. The reactor vessel thickness increases to 1" at the top, increasing the outer diameter to 60"; from this, the total centerline length of the volute can be calculated as 201.28" [16]. The flow path of this region is shown below in Figure 6.

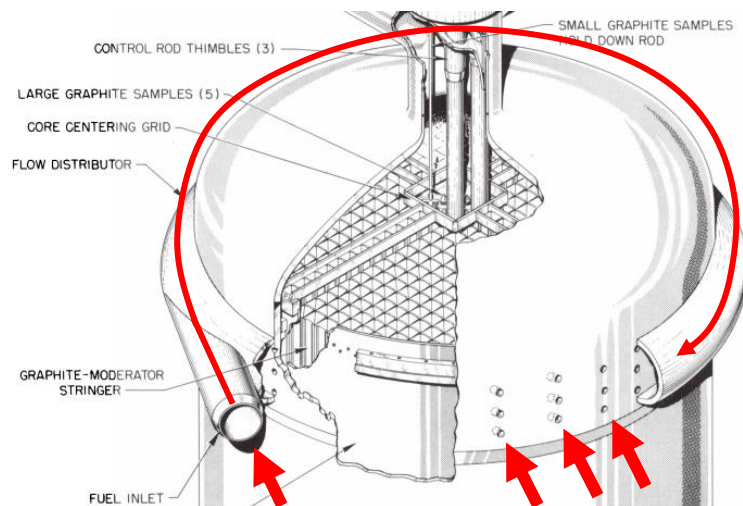


Figure 6: Inlet Distributor and Distributor Orifices Flow Path

The incoming fuel salt enters the gap between the reactor vessel and the core can – the cooling annulus - from the volute through a series of orifices drilled into the reactor vessel. Each orifice is 0.75" in diameter and occur in vertical stacks of 3 along the length of the volute, with a total of 84 orifices [37]. The orifices start at the volute entrance and the stack spacing is 5 degrees

around the circumference; the stacks increase to 22.5° at the tail of the volute, due to the increasing pressure and velocity along the length of the volute. This evenly distributes the salt into the annulus. The orifices are angled at 30 degrees to the tangent to impart spiralling flow as it enters the annulus [16, p. 75].

The flow enters the 1" gap between the reactor vessel and core can, referred to as the cooling annulus. The total height of the annulus is approximately 56.75" from the entrance to the lower plenum as calculated from Figure 7; however, due to the spiral nature of the flow from the volute, the actual path travelled by the fluid is much longer.

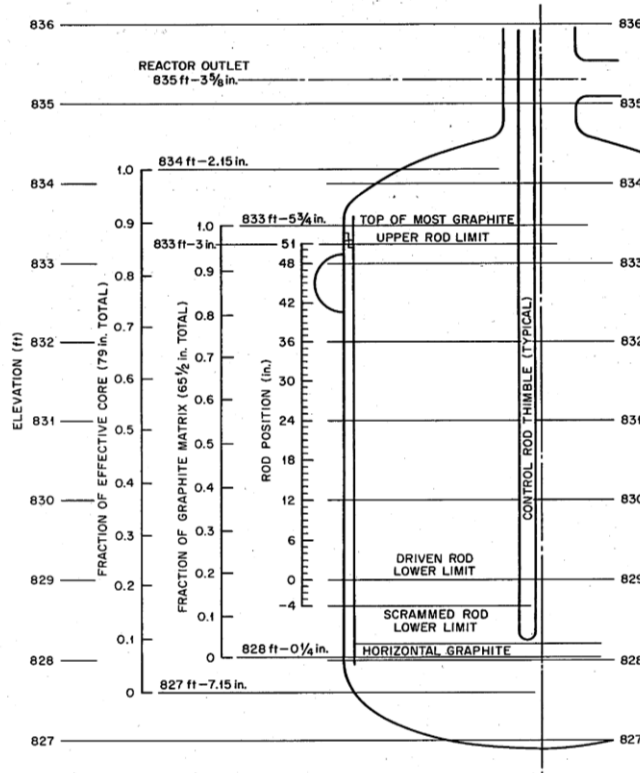


Figure 7: Elevation of MSRE and Select Internal Components

The flow path of the cooling annulus is shown below in Figure 8, illustrating the spiralling nature of the flow after it passes through the distributor orifices.

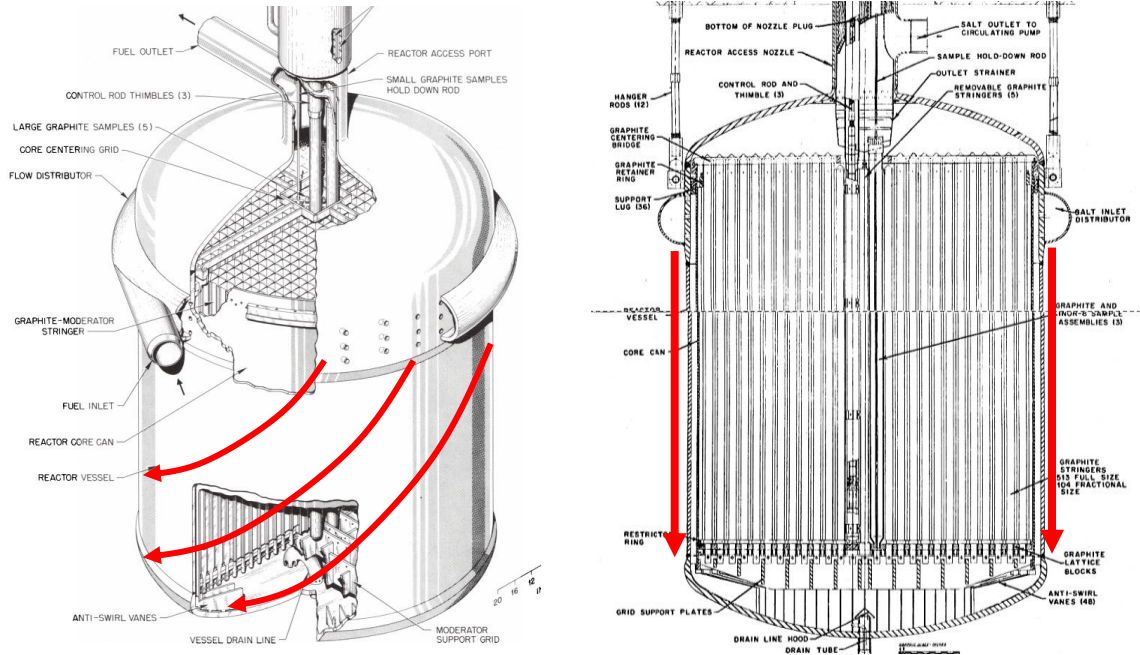


Figure 8: Cooling Annulus Flow Path

Kedl's hydraulic experiment measured a number of parameters in this region. The inlet velocity through the 5" pipe was 19.2 ft/s, while the velocity through the volute ranges from 23 ft/s at the entrance to 10 ft/s at the tail, as seen in the results in Figure 9. The sudden jump in velocity at the entrance is due to recirculation in the volute where the tail connects to the entrance.

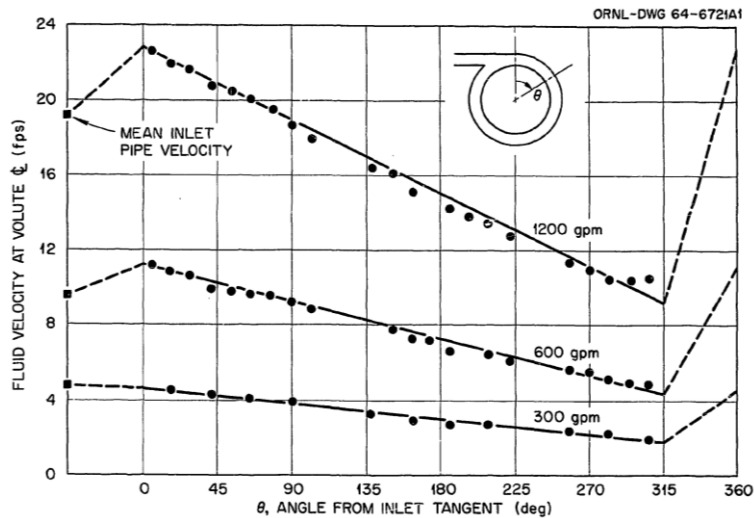


Figure 9: Volute Centerline Velocity as a Function of Angle [37]

The velocity through the orifices range from 4 ft/s at the entrance of the volute to 18 ft/s at the tail [37]. Figure 10 shows the fluid velocity along the annulus; at a flow of 1200 gallons per minute, the velocity at the bottom of the cooling annulus is 5.5 ft/s. This is in disagreement with

the value reported by Robertson of 4.2 ft/s – since this was only reported as a single value, it was assumed the value was superseded by the more recent Kedl experiment paper [16, p. 96].

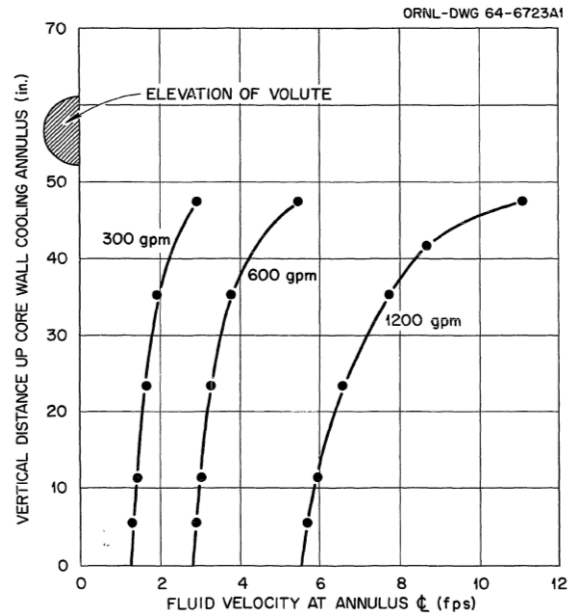


Figure 10: Annulus Centerline velocity along the Annulus Length [37]

3.3.2 Lower Head

The flow exits the cooling annulus and enters the lower head through 48 radial anti-swirl vanes, designed to straighten the flow as it enters the lower head. The vanes are 0.125" in thickness, starting at the edge of the reactor vessel and extending inward 11" [16]. The spacing between the vanes was calculated to be 3.67" at the vane inlet and 2.23" at the outlet; the height of the vanes vary due to the shape of the reactor vessel head.

A 1.5" schedule 40 drain line extends 2.75" into the lower head [37]. It is capped with a conical umbrella to prevent particulates blocking the line during draining. The design and assembly of the anti-swirl vanes and drain can be seen in Figure 11.



Figure 11: Assembly of Anti-Swirl Vanes and Drain Line in the Lower Head [42]

The graphite assembly sits on an INOR-8 support structure, a grid composed of 0.5” thick plates set on edge and fastened to the bottom of the core can so that it moves as the components expand with temperature rise [16]. The height of the grid varies from 1.625” at the core edge to 5.5625” at the center, due to the slope of the straightening vanes. While no other details about the geometry of the plates or assembly of the grid were found, it can be seen in Figure 1 that the plates in one direction are shorter than the other, seemingly to accommodate the rods used to hold down the graphite stringers (see Section 3.3.4 Core). Additionally, Figure 2 shows that the central region has closer grid spacing due to the center graphite stringers and control rods being supported directly by the INOR-8 grid, further discussed in the following section [16, p. 84]. This can be confirmed in Figure 12. Figure 2 also seems to show the spacing to allow for the dowel ends of the graphite stringers, though this image is not to scale so may be misleading. Overall, this region has little impact on the flow as the spacing is large – the 19-region model developed by Engel and Haubenreich for neutronics study provides a volumetric fuel fraction of 90.8% for the region [45].

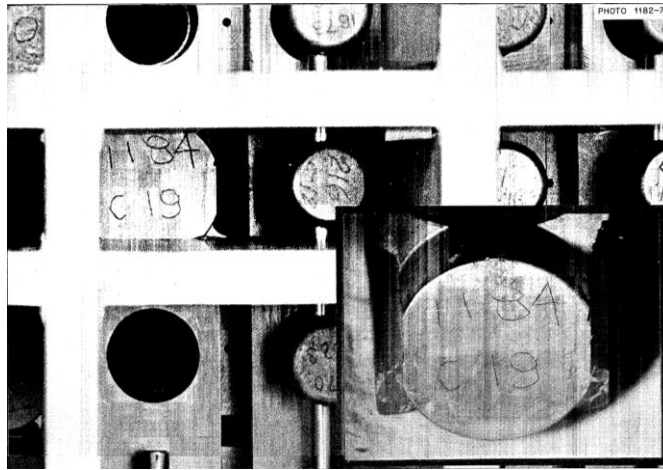


Figure 12: Image from the INOR-8 Support Grid and Dowels in the Lower Plenum [47]. The main image is before MSRE operation, and the bottom right image is after operation.

The pressure along the wall of the lower head was measured and plotted in Figure 13. The pressure is slightly higher in the center due to some remaining swirl entering the lower plenum. While the anti-swirl vanes greatly reduce the swirl in the lower head, they also produce a high velocity stream along the wall which was measured separately [37].

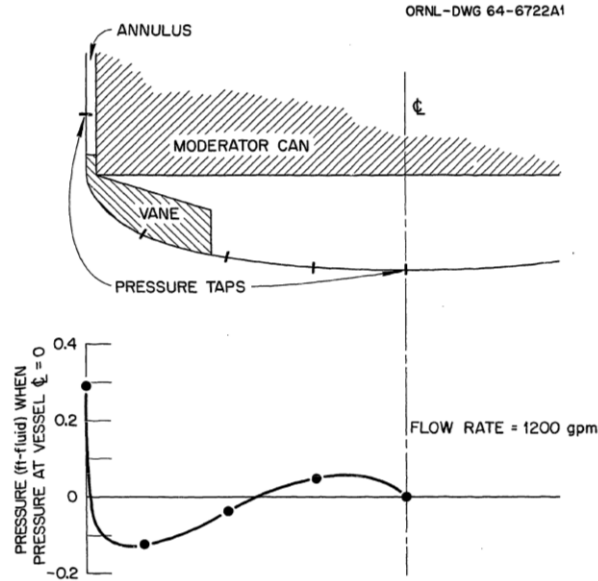


Figure 13: Lower Head Radial Pressure Gradient [37]

The velocity through the INOR-8 support grid was measured to be 0.16 ft/s [16].

3.3.3 Graphite Lattice Support Grid

Between the INOR-8 structure and the graphite core is a graphite support grid. The graphite grid consists of two layers of perpendicular rectangular graphite bars; each bar is 1" in height and 1.625" wide [37]. This produces small square passages through the grid of 0.375" width. Initial tests of the grid and core showed that fuel salt channels directly above the graphite grid were starved of flow compared to channels over the gap, which was partially corrected by drilling additional orifices of 0.104" diameter in the top bars under those channels. The geometry of the grid and orifices in relation to the channels is displayed above the channel flow rates in Figure 17 below; it is noted that this data was corrected to account for the additional drilled holes, though how this correction was done was not specified.

The grid is discontinued at the center, where the center 5 graphite core blocks are, to allow for greater salt cooling past the control rods and specimen holder are located. This effects approximately 16 channels, with a few others minorly effected. At the overlap of the bars, holes with a taper and a minimum diameter of 1.040" accept the doweled ends of the graphite stringers that make up the core [16].

Kedl's hydraulic experiment test determined the majority of core pressure loss occurs through the graphite due to the small flow clearance area. The fluid had a velocity of 4.5 ft/s, and as can be seen in Figure 14, the head loss measured across the grid was 0.51 ft-fluid [37]. The pressure loss across the grid alone was measured in a separate experimental setup.

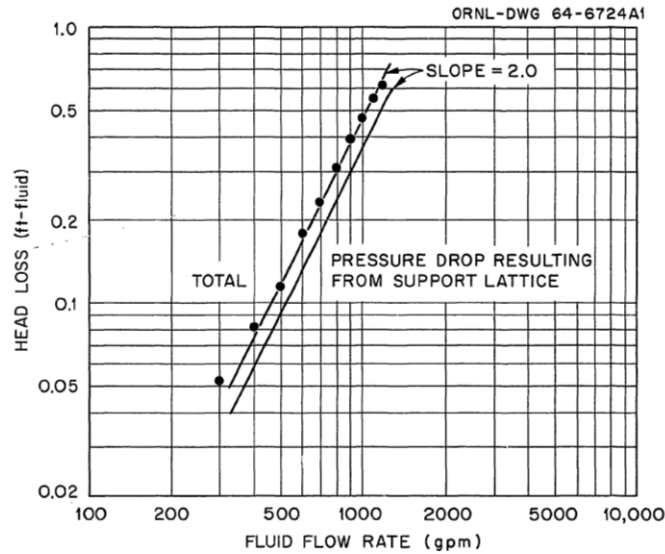


Figure 14: Experimental Head Loss through the Graphite Support Grid and Core [37]

3.3.4 Core

The graphite core is composed of square graphite stringers, with grooves cut into the sides to form channels for the fuel salt to flow. This creates 1140 full-size equivalent channels [37]. The geometry of the stringers can be seen in Figure 15; stringers have a pyramid shaped top to prevent salt from pooling when the reactor is drained. Using information in the 20-region model [49], the bulk length of the stringers are 62.59", with the pyramidal top section being an additional 2.94" in length [45] [49] [50]. This matches with the elevations in Figure 7, and [40] [16, p. 79] which lists the total stringer length at 67" when the dowels are added. However, this conflicts with Figure 15 which lists the total length as 63", as well as [16, p. 84] which lists an average stringer length of 62.125". Additionally, the central 5 graphite stringers sit directly on the INOR-8 support structure and are 64.5" in length, and were fitted with lifting knobs instead of the pyramid shape top to allow their removal [16] [47, p. 139]. Part of the discrepancy may be due to the graphite stringers along two perpendicular centerlines of the reactor being longer, as can be seen in Figure 3; no information on the length of these or the reason for these longer stringers was found. It was assumed these were to properly align the core with the centering bridge.

A 1.2" diameter disc at the bottom of the square portion of the stringer sits on top of the graphite grid. While no dimension for their height was found, Figure 2 and images of the as-built core found in [42] indicate the discs are the same height as the restrictor ring, which is 0.5" and discussed below [16].

The bottom dowels pass through holes in the graphite lattice and have contain a bushing in a 0.375" diameter hole. A 0.3125" diameter INOR-8 rod passes through this hole and a corresponding hole in the INOR-8 grid structure to prevent the graphite assembly from floating during operation. The dowels are 1" in diameter and extend 1.41" below the graphite grid, yielding a total length of 3.41" [16] [49].

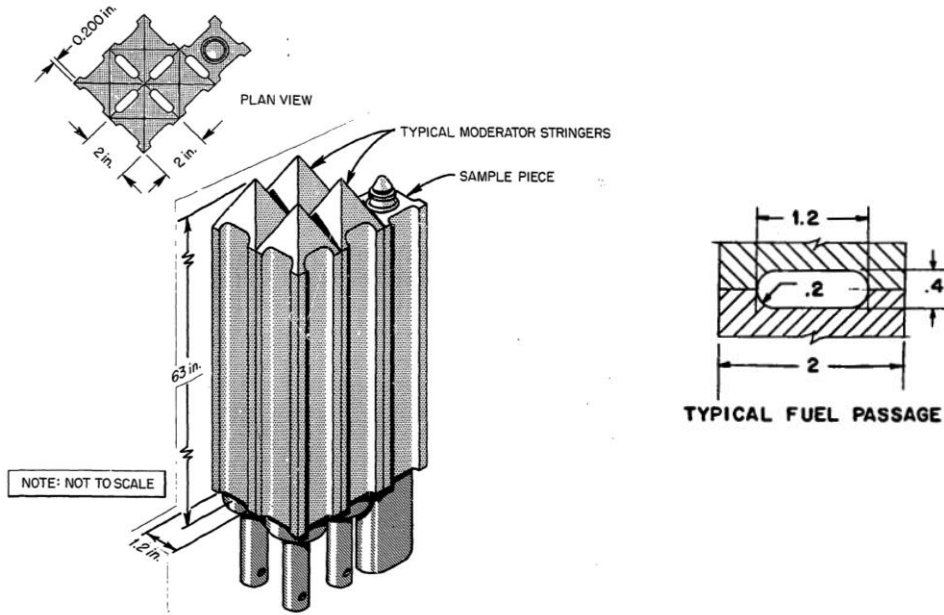


Figure 15: Graphite Core Stringer Geometry and Channel Dimensions [16]

The center of the core contains 3 control rods and a removable sample basket, as shown in Figure 16. The control rod thimbles are fabricated from 2" schedule 40 INOR-8 pipe [16]. In the hydraulic experiment, these elements were not present as they were still under development – the regular graphite matrix was continued in this region [37]. As such, these items are not discussed in more detail here, though extensive information is available in [16]. Stringers labelled 7, 60, and 61 in Figure 16 were removable and sit directly on the INOR-8 support structure.

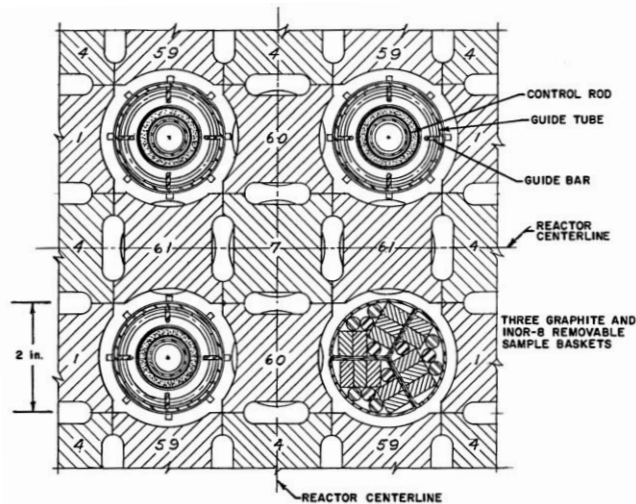


Figure 16: Control Rod and Sample Basket in Core [16]

A small gap exists between the core can, with an inner diameter of 55.5", and the graphite core, with a nominal diameter of 55.25". An INOR-8 restrictor ring with dimensions 0.5"x0.5"x54.5" (inner diameter) was placed around the disc at the bottom of the stringers to limit the flow in this

gap as the components expand during operation, and to restrict the core stringers from movement.

The pressure drop through the core was measured and is displayed above in Figure 14 to be approximately 0.1 ft-fluid. The velocity of the fluid through the bulk channels was 0.7 ft/s, and the flow rate was measured through randomly selected channels and is displayed radially in Figure 17 [37]. There is significant scatter of data due to the large tolerances in the graphite grid in the hydraulic experiment, as well as a decrease in flow with radius due to the pressure gradient in the lower head.

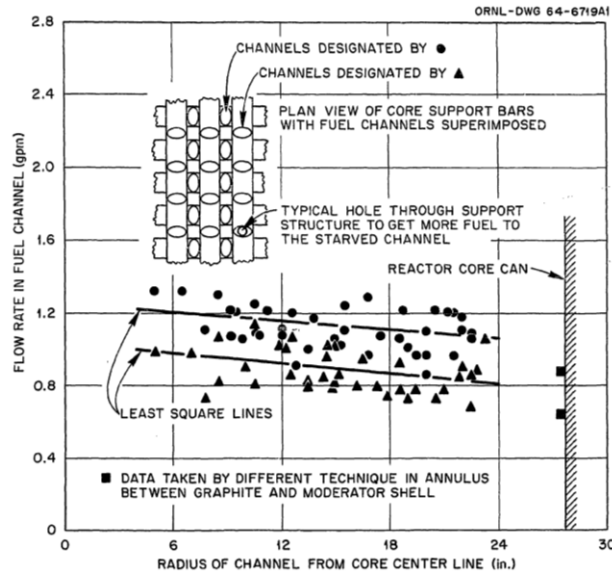


Figure 17: Experimental Core Channel Flow Rates [37]

The 16 central channels - where the graphite grid was discontinued - was measured separately. Two different techniques were used; the first measured an average flow rate of 2.3 gallons/minute, while the second measured 3.6 and 3.7 gallons/minute [37]. Since this was adequate for cooling, no attempts were made to investigate this discrepancy. Engel and Haubenreich [45] report 43 gallons/minute total for the region for the MSRE, though this is in the same report as the 5-region model which also reports 72 gallons/minute through the center region. It is noted that this value would be with the 4 central thimbles; a review of the flow area differences may clarify this issue. The central channels are reported to have a velocity of about 3 times the average channel velocity [16], yielding 2.1 ft/s, and velocities were estimated to remain the same with the control rods and sample holder present [37].

Two data points in Figure 17 are in the gap between the core and core can. These data points were actually the “flow rate corresponding to the measured pressure drop in a standard fuel channel” [37, p. 24], as the exact hydraulic parameters were unknown. It was assumed that this statement indicates the flow through the gap is proportional to the area; thus, with the average between these two data points of about 0.78 gallons/minute, the total flow through the gap can be calculated:

$$Q_{gap} = \frac{A_{gap}}{A_{channel}} Q_{channel}$$

$$Q_{gap} = \frac{21.746''}{0.446''} (0.783) = 38.2 \frac{\text{gallons}}{\text{minute}}$$

3.3.5 Upper Head and Outlet

The fluid exits the core channels into a shared volume, similar to the lower head. The flow then exits the reactor through a 10" schedule 40 pipe, with a branch that reduces to the 5" schedule 40 outlet pipe about 10" along the tee length [16] [40]. The through-flow section of the tee contains a plug to prevent fuel salt from entering but to allow the feedthrough of the control rods; the small gap between the 9.770" outer diameter of the plug and the pipe is blocked with frozen fuel salt [16]. The tee is contoured to direct flow to the 5" exit, as shown in Figure 18.

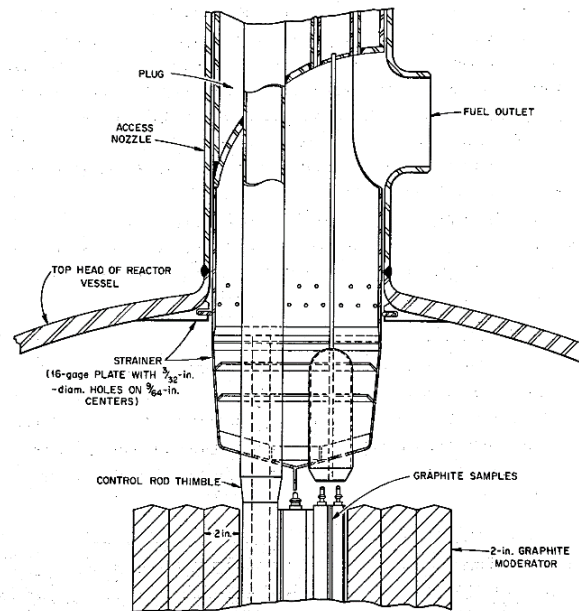


Figure 18: Upper Head and Outlet Geometry [40]

A strainer assembly was added to the core, the top of which appears to be attached to the flow contouring device. This strainer was not present in the hydraulic experiment but was not anticipated to change the flow significantly [37]. This strainer assembly protrudes into the upper plenum and was installed to catch any pieces of graphite that may become loose during operation. A small cross-shaped structure was added to the bottom to hold down the center 5 removable stringers [16]. Detailed geometry and drawings of the components are listed in [16] [40] but are not included here as they do not impede flow. The flow area of the 10" pipe is reduced by 19% due to the three 2.5" diameter control rod thimbles [40]. Due to the lack of strainer assembly and control rods in the hydraulic experiment, it is assumed there is also no flow contouring device. Figure 4 supports that the outlet component was a blanked off non-standard tee in the hydraulic experiment [37]. Additionally, the image indicates that the 5" outlet

was about 20" above the reactor vessel in the hydraulic experiment, much higher than the 10" reported for the MSRE [40]. It appears the distance from the tee to the pressure sensor in the hydraulic experiment is approximately 22" in length.

A centering bridge sits on top of the graphite stringers to prevent excessive movement; no dimensions of this component or the reference drawing were found [16]. As this component has no effect on flow, it was subsequently ignored.

The velocity in the upper plenum was measured using fluid age technique using probes along assumed streamlines [37]. As can be seen in Figure 19, the velocity is multi-dimensional.

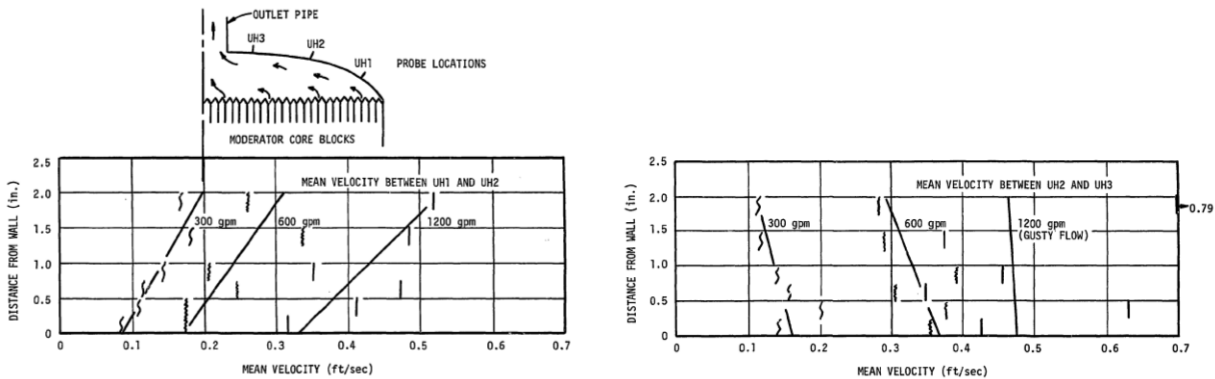


Figure 19: Upper Head Experimental Velocity Profile [37]

3.3.6 Upper Plenum Short Circuit

The core can attaches by its flange to the reactor vessel through a series of 36 lugs welded to the reactor, as shown in Figure 20 [16]. To prevent a stagnant region above the core can flange, 18 small channels 0.2"x0.2" were cut into the can flange at an angle of 30 degrees to allow some salt to bypass the core and directly enter the upper head from the cooling annulus.

Kedl [37] lists the flow to be 25-50 gallons/minute depending on tolerances. It is unclear if this short circuit was present in the hydraulic experiment, though from the experimental results it is assumed that the fuel short circuit was added afterwards. Robertson [16] notes about 24 gallons/minute of flow is diverted this way. It is also mentioned that 3-22 gallons/minute would pass through the annular clearances at the core can support flange, which was assumed to be the same region and brings the value in line with Kedl [16, p. 85]. Unfortunately, the reference document for this value could not be found, and no mention of the fuel short circuit could be found in the semi-annual progress reports.

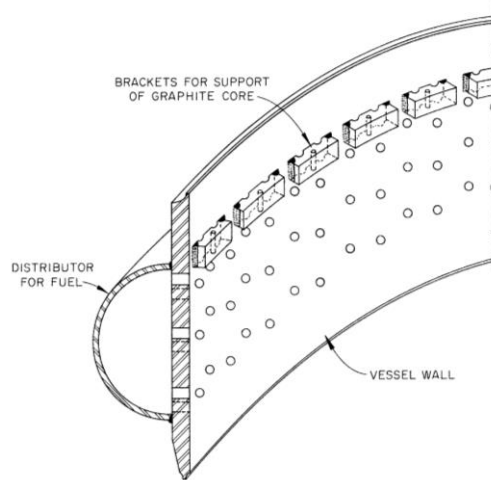


Figure 20: Reactor Vessel Lugs above Volute Orifices [51]

3.4. Thickening Agent Studies

The majority of tests run with the hydraulic experiment used water as the fluid, resulting in a Reynold's number approximately four times greater than would be expected with molten salt [37]. Certain tests were also done on the hydraulic model with low concentrations of the thickening agent Jaguar-508 to match the expected Reynold's number of molten salt.

Limited information was provided on these experiments, except to confirm a handful of observations of the water experiments. Throughout the experiment, it was found that the volute, lower head and upper head had high Reynold's numbers, so would exhibit the same flow patterns in the full MSRE. The heat transfer coefficient in the lower head was calculated and found to be equal with and without the thickening agent added.

No other documents found referenced the thickening agent tests. As the few results available indicate that matching the Reynold's number did not effect results of the test in question, no attempt to include these results in the Flownex model were made.

4. Flownex Simulation Environment Model

Flownex Simulation Environment is a 1-dimensional system level code for simulating heat transfer and fluid dynamics in a variety of industries and applications, including nuclear reactors. Flownex originated in 1986 as an air and water network solver for mining operations, and was updated in 1999 to simulate the Pebble Bed Modular Reactor [52]. It also has ongoing development and support. Flownex has a variety of features that make it desirable for thermalhydraulic analysis; the most obvious is the graphic user interface, with 'drag and drop' capability for standard components and the ability to create custom components. Specific components for nuclear analysis are available, such as for pebble bed type reactors and neutronics scripts. Both steady state and transient simulations can be performed, and additional features include integration with Excel, Python, ANSYS and RELAP, among others useful software. Flownex also features an internal C# scripting environment that allows for excellent control over network creation and simulations. Finally, one of the most desirable features of Flownex is the ability to implement custom materials based on properties, making it ideal for simulating new reactor types.

4.1. Flownex Model Simplifications

Based on the geometric data summarized in Section 3.3, a number of simplifications must be made for both the complexity of the model and to accommodate for Flownex being a 1-dimensional code. This and the following section discuss any approximations or assumptions made to produce a Flownex model based on the known geometry discussed in Section 3.3.

- The volute uses only average values (half of the total volute length, average velocity) as only the total loss through the orifices is important. Thus, no recirculation occurs in the Flownex model, as the tail of the volute does not connect to the entrance.
- The cooling annulus is modelled as 1-dimensional, despite containing complex 3-dimensional flow.
- The anti-swirl vanes are modelled as conical expanding pipes; thus, no flow can exit the top of the vanes.
- The lower head contains complex 3-dimensional flow patterns that produces a pressure gradient, which could not be modelled [37] [53].
- The INOR-8 support grid was ignored due to its negligible effect on the flow and unknown geometry.
- The dowels protruding below the graphite grid were ignored; the dowel holes in the graphite grid were assumed to be completely filled with graphite. The channels were assumed to start directly after the graphite grid, ignoring the short disc that separated the grid and stringer. However, inlet losses to the channels were still calculated as normal.
- The pyramid heads of the stringers were ignored, as they did not impact the flow in the channels or upper plenum.
- The strainer basket at the outlet was ignored, as it was not in the hydraulic experiment and was assumed to have no impact on the flow [37]. The flow contouring device in the outlet tee was assumed to not be in the hydraulic experiment.

4.2. Model Input Data

Table 1 contains the input data for the Flownex model. Both the provided imperial dimensions and the dimensions in SI units are provided. All values below are directly from Section 3.3 or calculated from provided geometry values except where noted.

Table 1: Model Input Parameters Summary

Parameter	Provided Values (in)	Input (cm)
Core Height	62.59	158.98
Core Outer Diameter	55.25	140.34
Fuel Channel Area	0.446 in ²	2.88 cm ²
Graphite Grid		
Single Bar Dimensions	1x1.625	2.54x4.13
Grid Orifice	0.375x0.375	0.95x0.95
Drilled Correction Hole Diameter	0.104	0.264
Anti-Swirl Vanes		
• Inlet*	-	Circumference = 23.729 Area = 23.684 cm ²
• Outlet*	-	Circumference = 34.83 Area = 59.877 cm ²
• Length	11	27.94
• Number in Parallel	48	48
Core Can Inner Diameter	55.5	140.97
Core Can Outer Diameter	56	142.24
Reactor Vessel Inner Diameter	58	147.32
Cooling Annulus Height	56.75	144.15
Distributor Length	201.28	511.24
Distributor Orifice Diameter	0.75	1.905
6-inch inlet to Distributor, Length**	14.78	37.54
Fuel Short Circuit Total Clear Area	0.72 in ²	4.65 cm ²
*Height estimated based on provided figures		
**Estimated based on provided figures		

The core was split into 3 radial zones – the central 16 channels where the graphite grid was discontinued, the core bulk, and the peripheral channels. The central region has different hydraulic parameters, but the rest of the core can be split into as many regions as required for future neutronic studies or power distributions. The peripheral zone outer radius and number of channels was taken from the 5-region model, with the remaining channels assigned to the bulk [45]. However, based on the known geometry of the central region, the diameter of this region should be 3” plus the width of a channel of 0.4”, shown below in Figure 21. Since the hydraulic experiment has a continuous core without the control rod or sample holder, the porosity in the central region is approximately the same as the core bulk in the hydraulic experiment; this value would need to be updated to model the operating MSRE with control rods, as well as for the extra clearance in the graphite grid due to the unfilled dowel holes directly below these elements.

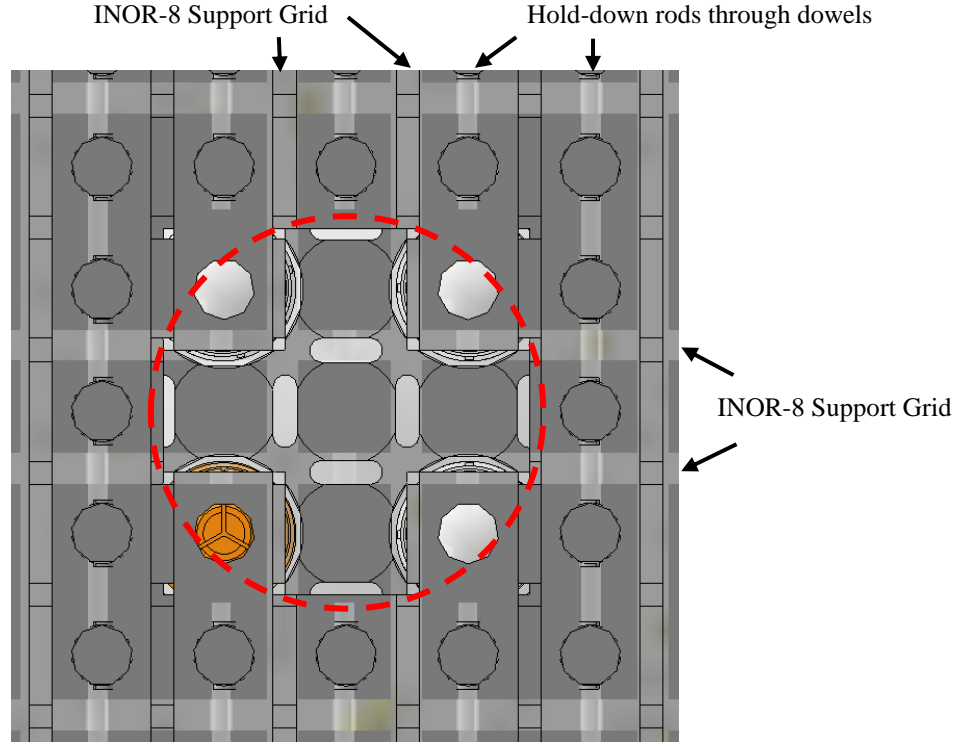


Figure 21: Bottom view of the central region of core and graphite grid. Light grey lines (not passing through dowels) represent the INOR-8 support structure [54]

A 6-region model, including the core, gap between the core and core can, core can, and downcomer was created for modelling in Flownex, as explained below in Section 4.3. The zones are described in Table 2.

Table 2: Hydraulic Model Core Input Geometry Parameters for Flownex Reactor Geometry Chart

Region	Inner Radius, cm	Outer Radius, cm	Total Zone Volume, m ³	Channels	Zone Permeability	Grid Orifice Volume, m ³	Grid Permeability
Core Center	0	8.128	0.033	16	0.2217	-	-
Core Bulk	8.128	66.294	2.162	1062	0.2245	0.002595	0.03756
Core Periphery	66.294	70.168	0.264	78	0.1351	0.000191	0.02259
Gap	70.168	70.485	0.022	0	1	0	1
Core Can	70.485	71.120	0.028	-	0	-	-
Cooling Annulus	71.120	73.660	0.116	-	1	-	-

The pressure loss through the system was calculated using the standard formula:

$$\Delta P = \left(f \frac{L}{D_h} + \Sigma K \right) \frac{\rho v^2}{2}$$

Where f is the friction factor from the material, L is the characteristic length, D_h is the hydraulic diameter, K is the minor loss coefficient, ρ is the fluid density, and v is the velocity. The inputs

for the minor losses of components are discussed below. While all major losses due to friction (the first term above) are calculated by Flownex, some corrections were made to the friction factor discussed in Section 4.2.2 Core Channel Major Loss.

4.2.1 Minor Losses

As will be discussed in Section 5.3, the minor losses were the dominant phenomena dictating the flow distribution in the MSRE hydraulic experiment due to the complicated geometry. Even some standard components, such as the reducing tee at the outlet, had assumptions associated with their losses as their size was outside that of regularly manufactured components. The majority of the losses were calculated using Idelchik [55].

The values reported below are the values calculated using the geometry and input assumptions to Flownex; the associated errors or tolerances on each element is discussed in Section 5.3. Many of the input minor loss calculations rely on the velocity through the component; all values for this model were calculated with a flow rate of 1200 gallons/minute, as the majority of the data presented by Kedl for the hydraulic model used this flow rate. To increase the usefulness of the model, the minor losses could easily be calculated with a C# script in Flownex to compare the model to the experiment at different flow rates; script calculation of losses would also be required to model transient behaviour in the full MSRE, as discussed in Section 6.1.

Inlet Piping and Distributor

This region includes the entrance to the volute from the 5" inlet pipe to the 6" volute inlet, the volute circling the perimeter of the vessel, and the orifices between the distributor and the cooling annulus. These regions are shown for both the reactor geometry and the Flownex model (discussed below) in Figure 22.

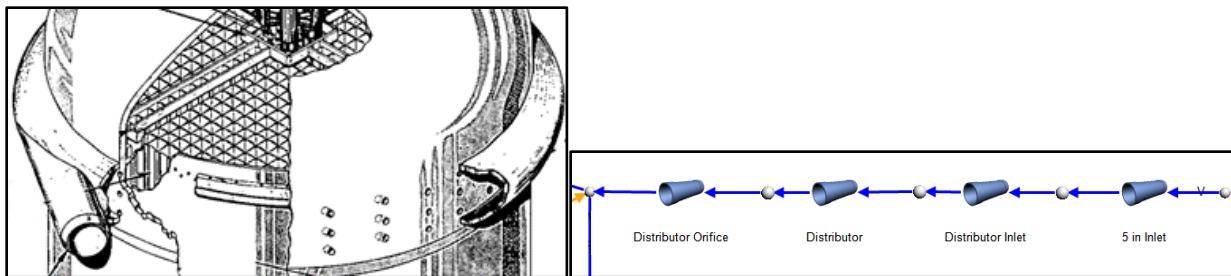


Figure 22: Inlet, Volute (Distributor), and Orifices of the MSR (Left) and Flownex Network (Right)

The expansion from the 5" inlet pipe to the 6" pipe at the start of the volute is only based on a ratio of areas, and was calculated to be $K=0.1$ [55, p. 246] [56, p. 436].

The slight reduction from the 6" pipe to the volute was calculated as a standard sudden contraction. This is also only based on area ratios, and yielded $K=0.089$ [55].

The entrance to the orifices is complicated, as the velocity changes along the length and the orifices themselves occur in stacks of 3 and at a 30° angle to the tangent [37]. Idelchik provides loss calculations for orifice stacks in a thin plate with passing flow; however, this doesn't

account for the orifice angles or the fact the orifice wall is 1" thick, though no restriction on wall thickness was provided [55, p. 268] [16]. The loss for this case was calculated as $K=3.13$ and was the value used due to the lack of more accurate data. This case also exists for baffled orifices, but only for baffles directed against the flow inlet and not into it. While Idelchik also provides losses for angled entrances in passing flow, the K values would fluctuate dramatically along the length of the volute as the velocity ratio of passing flow to orifice flow decreases dramatically and the orifice flow is not precisely known [55, p. 194]. An additional method to calculate this value would be to assume the geometry of a header; calculations either required branches at 90° [55] or required some knowledge of flow rates and losses to iterate a solution [57, p. 358], which would also require large degrees of approximation. No calculations or experimental results for a ring style manifold could be found, which would match this application well.

Anti-Swirl Vanes

The anti-swirl vanes reside in the lower plenum; the flow must pass through them after the cooling annulus. A zoomed in view of this region from Figure 1 can be seen in Figure 23.

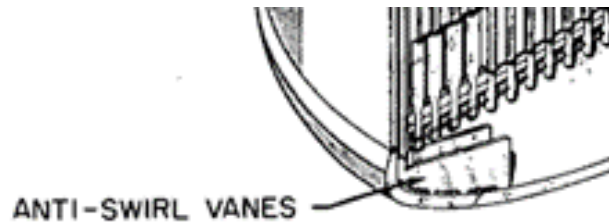


Figure 23: Zoom-in of Anti-Swirl Vane Region

The anti-swirl vanes contain an entrance where the cooling annulus ends, a curved expansion as the cross-sectional area of the vanes change as their height varies along the curved bottom head, and an exit to the lower plenum. As mentioned previously, the vanes were modelled as a pipe with changing cross section, so no flow exits the top of the vanes. A relation for a curved diffuser was employed, finding $K=0.496$, though the experimental results varied by $\pm 20\%$ [58]. It is important to note that this loss uses the entrance velocity, which was employed with the Flownex feature to use the K value based on minimum area. The calculated pressure loss agrees fairly well with the loss calculated assuming the curve is a 105° angle elbow and using the average velocity. The entrance loss to the vanes was modelled as a square entrance to a conduit between two walls with $K=0.71$ [55, p. 202]. The exit is a standard exit to an unrestricted volume; however, the standard $K=1$ value had to be scaled with the ratio of the inlet and outlet velocity of the expansion, yielding a scaled value of $K=0.1565$. The total K value of this section is $K=1.36$; since the component attenuates the 3-dimensional swirl flow pattern, this value could be larger in reality.

Graphite Grid and Core

The graphite grid was approximated as a thick orifice plate [55, p. 594]. This was seen as a reasonable approximation as an orifice plate was used in the original 1/5 scale experiment to replicate the flow pattern [59, p. 27]. The loss calculation relies on several parameters and uses the inlet velocity to the plate; since Flownex uses the velocity within the orifices to calculate the

losses, the value was scaled by the velocity in the lower head [60]. The calculated value used in the model was $K=1.65$. It is noted that the calculated velocity through the graphite grid is lower than the measured value in the hydraulic experiment, which would lead to a lower K value.

The 0.5" support disc was not included in the model, as the region has a complex geometry that could not be accurately modelled with existing data. The region is very small and would add to the turbulence of the flow due to the expansion from the graphite grid immediately into the core channels.

The inlet to the bulk of core channels posed a unique challenge, as the graphite grid directly before the channels causes significant turbulence before the flow enters the channels. This has been shown to have significant changes to the flow and friction factor and is heavily dependent on geometry [61] [62] [63]. Additionally, the channels are neither circular nor rectangular, which represents the majority of experimental values available in literature. The entrance loss was measured to be $K=2.3$ for a 3:1 aspect ratio rectangular duct at a similar Reynold's number, though it is noted that this was for a smooth inlet and thus the flow at this Reynold's number was still laminar despite being at a similar Reynold's number [64]. Other reported values ranged from $K=1.186$ to $K=2.8$, though these were for lower laminar Reynold's numbers [65] [66]. This geometry issue is subject to further discussion below in Section 4.2.2 and Section 5.3.

The inlet to the central core channels also contains a complicated geometry. As can be seen in Figure 21, the INOR-8 support structure blocks the passages where the graphite grid is discontinued. Additionally, it was unclear if the central channels still sat directly on this grid in the hydraulic experiment, as there were no control rods or sample holder. The minor loss to the inlet of this region was thus determined by matching the measured flow rate and provided velocity [37] [16]. The minor loss coefficient is $K=1.03$.

The outlet loss for the core is $K=1.23$. It has been found that the accepted exit loss of $K=1$ is true for large Reynold's numbers, but at low Reynold's number just outside the transition region the value is slightly higher [67].

Core Can Gap, Outlet, Fuel Short Circuit

The core can gap is the small region between the outside of the graphite core and the inner diameter of the core can; it has a restrictor ring that sits on the graphite grid to reduce the flow. The fuel short circuit is immediately above where the flow exits the volute orifices. Some of the flow in the cooling annulus goes upward past the core can mounting flanges and directly into the upper head. The outlet is the reducing tee, from 10" through the 5" branch, as the through-path of the tee is capped. These regions are shown below in Figure 24.

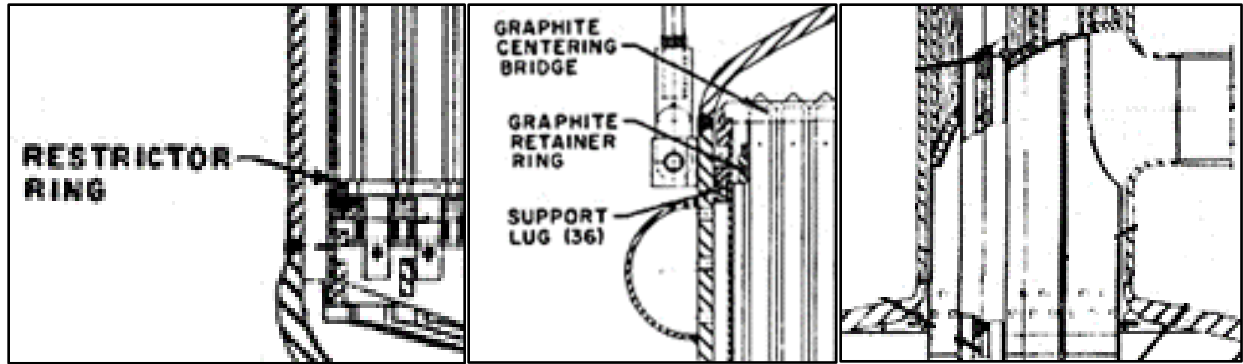


Figure 24: Zoomed-in MSRE Regions: Core-Can Gap (Left), Fuel Short Circuit (Middle), and Outlet Tee (Right)

The restrictor ring in the annulus between the core and core can has a provided geometry, but no details on exactly how it sits in the annulus. In the hydraulic experiment testing, it was stated that the exact hydraulic parameters were unknown; thus, the loss coefficient was also determined to match the experimental data for this region [37]. The value that matches the flow rate is $K=107.37$.

The exit of the core goes from the plenum through a 10" pipe, which has a standard inlet loss of $K=0.5$. The flow exits through a 5" side branch; while the MSRE contains a contouring assembly to direct flow to the side branch, seen in Figure 18, the assembly did not seem to be present in the hydraulic experiment. The tee was blocked at the through-run - in the MSRE this was by a plug, and in the hydraulic experiment by a blank flange. A lack of data is available on reducing tees, especially for large diameters and dead runs; studies have shown that reducing tees can be approximated by the sum of the loss of an elbow and a reducer, though the actual value is fairly dependent on the geometry and may actually be larger than the sum [68]. Miller provides a value of approximately $K=2.4$ for a branch to run tee ratio of 0.5 and 100% branch flow, though the value is slightly reduced to about $K=2.2$ with a fillet on the tee [57, p. 318]. These loss values were calculated using a ratio of the velocities, yielding a scaled value of $K=16.92$ for a non-filleted tee to obtain the same loss using the velocity in the 10" pipe as is used in Flownex.

The fuel short circuit was modelled as a pipe with a cross-sectional area equal to the sum of the 18 0.2"x0.2" slots that were machined into the flange [16]. Since these slots are on a 30° angle and sit in an unknown location on top of the core can support flange shown in Figure 20, which have their own non-standard geometry, the loss was calculated in the same way as the core-to-can gap. Since the actual amount of flow through this component was given as a range, the flow rate of 25 gallons/minute was matched as discussed in Section 3.3.6 Upper Plenum Short Circuit. A value of $K=0.168$ was calculated.

4.2.2 Core Channel Major Loss

The core channels present a challenge to model, as their unique geometry has no matching experimental data. The rectangular portion of the channels are a 2:1 aspect ratio, with semi-circular ends; if the entire channel is assumed to be rectangular, the aspect ratio is 3:1 [37]. Flownex assumes fully developed flow in all pipes in the system; effects such as developing flow, entrance effects, or friction factor changes must be accounted for manually [60]. These

effects are described below, as it was observed that entrance effects persist far into the channel length [42]. Most supporting research of different channel shapes are for square or rectangular channels, and there is little data on the transition flow regime of $2000 < \text{Re} < 10^4$, making accurate correction factors for losses challenging to predict. The biggest unknown effect related to the channel geometry is due to the vorticity caused in the corners formed by right angle walls, which would be mitigated to an unknown degree by the rounded ends in the MSRE channels [69] [70]. This effect is also worse for lower aspect ratio channels, such as those found in the MSRE.

While the terminology used here is typical for developing flows, it is noted that the Reynold's number of the channels is on the edge of the transition regime, as discussed below; the majority of the turbulence actually originates from the graphite grid. Thus, the observed entrance length effects are more akin to a wake effect, with the induced disturbances decaying along the length. It is unclear if the flow would fully re-laminarize without more detailed experiments or CFD analysis. It is also noted that these effects would have a substantial effect on heat transfer.

Effect of an Obstruction on Downstream Flow

Directly before the channel entrance is the graphite grid, which causes substantial turbulence and creates the majority of loss in the graphite. It has been shown experimentally that a downstream obstruction has significant effect on the flow pattern caused by vortices behind the obstruction, and causes an earlier flow regime transition and slight increase in friction factor [62] [63]. These effects are impossible to quantify for the MSRE, as it is primarily affected by the geometry of the obstruction, but are factored into the sensitivity studies in Section 5.3.

Critical Reynold's Number (Transition Region)

The Reynold's number of approximately 4300 in the bulk channels would normally be just beyond or in the transition region between laminar and turbulent flow; Flownex imposes a linear interpolation for friction factor values when $2300 < \text{Re} < 5000$. The inlet type and channel geometry impacts the flow regime, with transition occurring at $\text{Re}_{\text{crit}} = 1600\text{-}2800$ depending on the channel aspect ratio [64] [69]. The transition occurs earliest with an abrupt inlet, but with a rounded inlet $\text{Re}_{\text{crit}} = 5000$ for a square duct [64]. The value increases with increasing aspect ratio, but the flow should clearly be in the turbulent regime given the channel $\text{Re}=4300$ and the inlet obstruction increasing turbulence.

Entrance Length

In typical flows through circular pipes, entrance lengths are fairly low, though there is significant disagreement on exact values. Entry lengths depend on if the channel entrance is abrupt or smooth, the Reynold's number, and the geometry (circular or aspect ratio for rectangular channels). Values for the entrance length for square or rectangular channels vary from $20 * D_h$ [69] to more than $80 * D_h$ [71]. The majority of these results do not quantify the losses due to the entrance lengths. Experimental results for induced swirl at the entrance of a circular pipe indicate that entrance lengths are in the vicinity of $50 * D_h$, but decreases as Reynold's number decreases [72]. The entrance length effects are included in the friction factor calculation below, as this is a major contribution to the loss with the MSRE total core length only being $84 * D_h$.

Friction Factor

It has been found that using the hydraulic diameter in standard friction factor calculations can underestimate the friction factor in rectangular ducts by as much as 12% [69]. It has been proposed that Blasius matches the turbulent regime for rectangular channels well [64]; however, a composite study analyzed many experimental results for various aspect ratios and found that $f \approx 0.04$ in a turbulent 3:1 aspect ratio duct [73]. This is an increase of about 10% from the calculated value using standard D_h .

The above result does not account for the increased friction factor in the entrance length. Khan [74] provides the friction factor along the length of a square duct for $Re=5 \times 10^4$, and found an entrance length of $50 \cdot D_h$. The effect of the entrance length was approximated for the hydraulic experiment channels by scaling the values from Khan to the friction factor for a 3:1 channel at $Re = 4300$ from Jones [73] - a fit of the data was then produced to interpolate or extrapolate friction factor values along the channel length. A friction factor multiplier was added to the Flownex model to account for the new friction factor and entrance lengths. It is noted that while Khan reported an entrance length of $50 \cdot D_h$, there is still a non-negligible friction factor increase in the experimental data past $57 \cdot D_h$ [74]. As the aspect ratio increases, so does the friction factor [73].

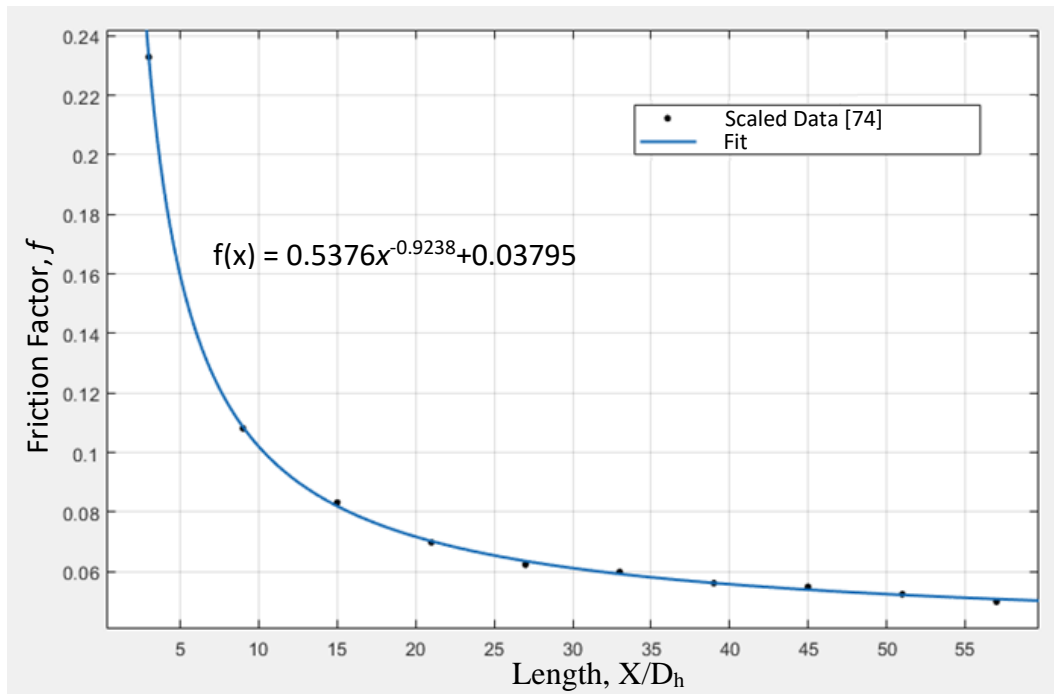


Figure 25: Scaled Experimental Data Estimating Entrance Length Friction Factors

Additionally, the decay of induced swirl at the entrance to a circular channel was previously experimentally studied at a variety of Reynold's numbers to investigate the impact on friction factor [72]. A similar exponential decay as reported by Khan was found; lower Reynold's numbers lowered the entrance length, and turbulence induced at the entrance of the tube had substantially higher entrance length friction factors than induced turbulence 6-12 hydraulic

diameters from the tube entrance. This experiment found that at a few hydraulic diameters, friction factor was 17 times greater than the fully developed friction factor, and did not decrease as rapidly as Khan's study. Due to the importance of channel geometry in this study, the scaled results from Khan were used, though it is likely that the true effect on friction factor is somewhere between these two studies.

This solution to the entrance length is not the recommended method for accounting for the entrance lengths. Rather, it is a rough estimate based on very limited available data of the possible effect the entrance length and channel geometry have on the frictional losses in the system. To accurately account for the MSRE channel geometry, experimental data or a CFD simulation should be obtained. The impact of the entrance length and frictional loss on the system is discussed further in Section 5.3.

4.2.3 Hydraulic Model Material Data

Flownex features the ability to add custom solids and fluids based on material properties, which is one of the main advantages over comparable codes for simulating new reactor types. This is especially convenient for MSR's, as there are many types of molten salts being investigated for potential reactor use.

The two materials in the hydraulic experiment are carbon steel and aluminum; no further information on the grade or type was provided [37]. As such, built-in materials from Flownex were used. For the core can, 'Carbon Steel – Plain Carbon' was used. 'Aluminum – Pure' was used for the graphite grid and core. For the fluid, 'H2O – Water' from the Pure Fluids database was selected.

Flownex pipe elements only carry fluid information, so no solid material is assigned. However, roughness values are required for major losses. Roughness values can be selected from the Flownex internal library, which contains some standard materials. For the carbon steel components, the normal value for Commercial Steel of 67.5 μm was used. For the aluminum components, an average value of 30 μm was used, which agrees with the internal value Flownex uses for aluminum ducting [60]. However, values for carbon steel range from 20-100 μm and 15-60 μm for aluminum [55]. The effect of this was investigated in Section 5.3.

4.3. Flownex Hydraulic Model

A full summary of the Flownex model inputs is available in Appendix A – Summary of Flownex Model Inputs.

4.3.1 Reactor Geometry Chart (RGC)

Flownex comes equipped with a tool for quickly creating full reactor geometries, called the Reactor Geometry Chart (RGC) [75]. This chart creates a full 360° axisymmetric core model based on inputs to a 2D chart, allowing different zones to be specified for different reactor sectors. The chart can then be used to automatically create a 2-dimensional network that can be modified or connected to other elements.

The RGC allows inputs based on 8 different zone types:

- Solid: Regions that have no flow, such as the core can. The roughness of the solid and the type of material can be specified.
- Single Cavity: A zone that has no solids material, such as the upper and lower head. Cavities can span multiple rows or columns, as adjacent Single Cavity zones are lumped together when creating the network. Single cavity zones must be used to connect to external systems, dictated by a 'P' in the zone shown in Figure 27.
- Solid with 1-D flow, horizontal or vertical: Used for solids with channels or permeability, such as the graphite core. The permeability of the zone, hydraulic diameter of a single channel, roughness, secondary losses and material can all be specified. Other parameters like the convection correlation can be specified with limited options but can be changed once the network is created.
- Horizontal or Vertical Cavity: These zones contain no solid and allow flow in a single direction, such as the cooling annulus or gap between the core can and core. These are kept distinct from adjacent cavities of the same type and create convection and radiation elements when the network is created, unlike the Single Cavity.
- Pebble Bed and General Fuel: These zones are not used for Molten Salt Reactors with liquid fuel. They allow zones representing solid fuel elements.

A colour-coded cross section of the MSRE is shown in Figure 26 illustrates how the hydraulic experiment was divided into zones for input to the Reactor Geometry Chart. The zone types and Reactor Geometry Chart for the MSRE is shown below in Figure 27. The red line in each image indicates the axis of revolution for the axisymmetric model.

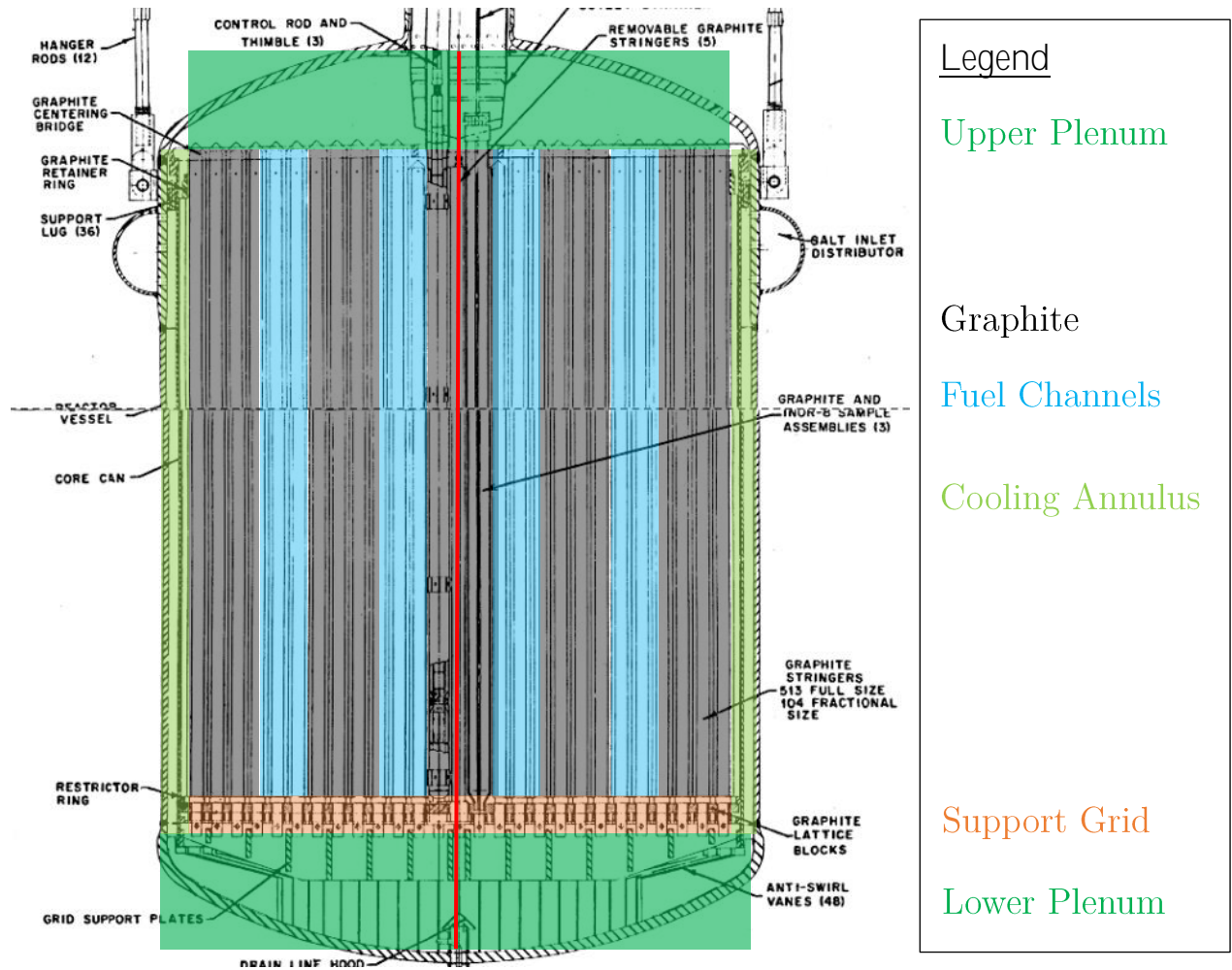


Figure 26: Colour-Coded Cross Section of the MSRE Core Indicating RGC Zones

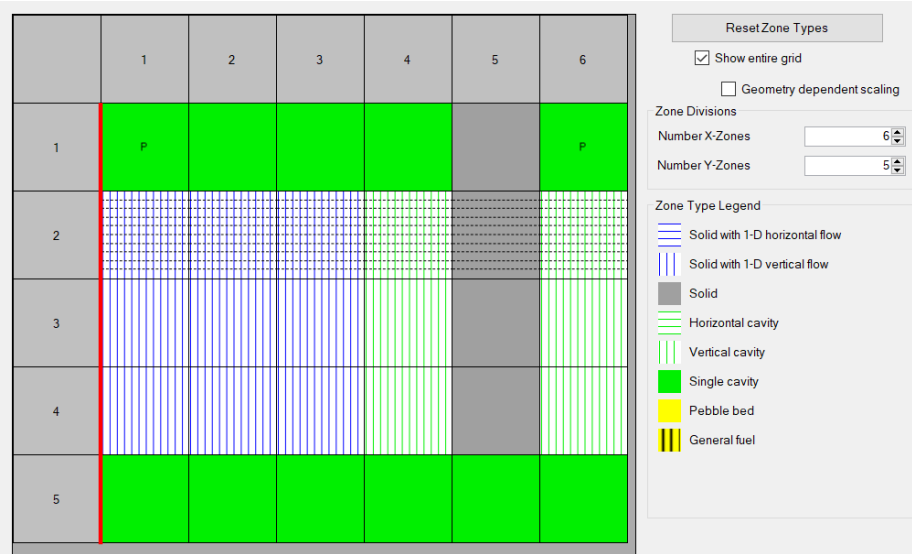


Figure 27: Flownex Reactor Geometry Chart for the MSRE Hydraulic Experiment

The columns in the chart represent the 6 zones described in Table 2, with column 1 as the core center, column 2 the core bulk, column 3 the core periphery, column 4 the core-can gap, column 5 the core can, and column 6 the cooling annulus. Thus, the axis of symmetry is to the left of column 1, with the core being ‘revolved’ around the core center.

Row 1 is the height of the upper head, and row 5 is the height of the lower head. Row 2 is the core; it has been further subdivided into 10 axial discretizations for increased fidelity. Row 4 in column 2 and 3 is the graphite grid. Row 3 has no physical significance; it is a thin boundary layer of 1 mm thickness, which is added at the recommendation of Flownex [76, p. 14]. This is because the generated network is a node-centered volume approach, with Pipe elements spanning adjacent zones in the Reactor Geometry Chart. Without this boundary layer, flow elements that span between the graphite grid and core have average values applied for certain parameters such as hydraulic diameter, leading to incorrect results. This layer has the same input parameters as the core layer above it so the correct values are used.

A full network can be automatically created from the Reactor Geometry Chart using the built-in Reactor Builder Script, creating flow paths, convection elements, conduction both axially and radially, and radiation elements where appropriate. After the network’s creation, additional elements such as the inlet and outlet pipes and volute were manually added to the network, as described below. A zoomed-in portion of the top and bottom of the network is shown in Figure 28, colour-coded to match the cross sectional Figure 26, with the red line representing the axis of symmetry. The full network is shown in Figure 29. The layer between the graphite grid and graphite core is the thin boundary layer, which has negligible volume.

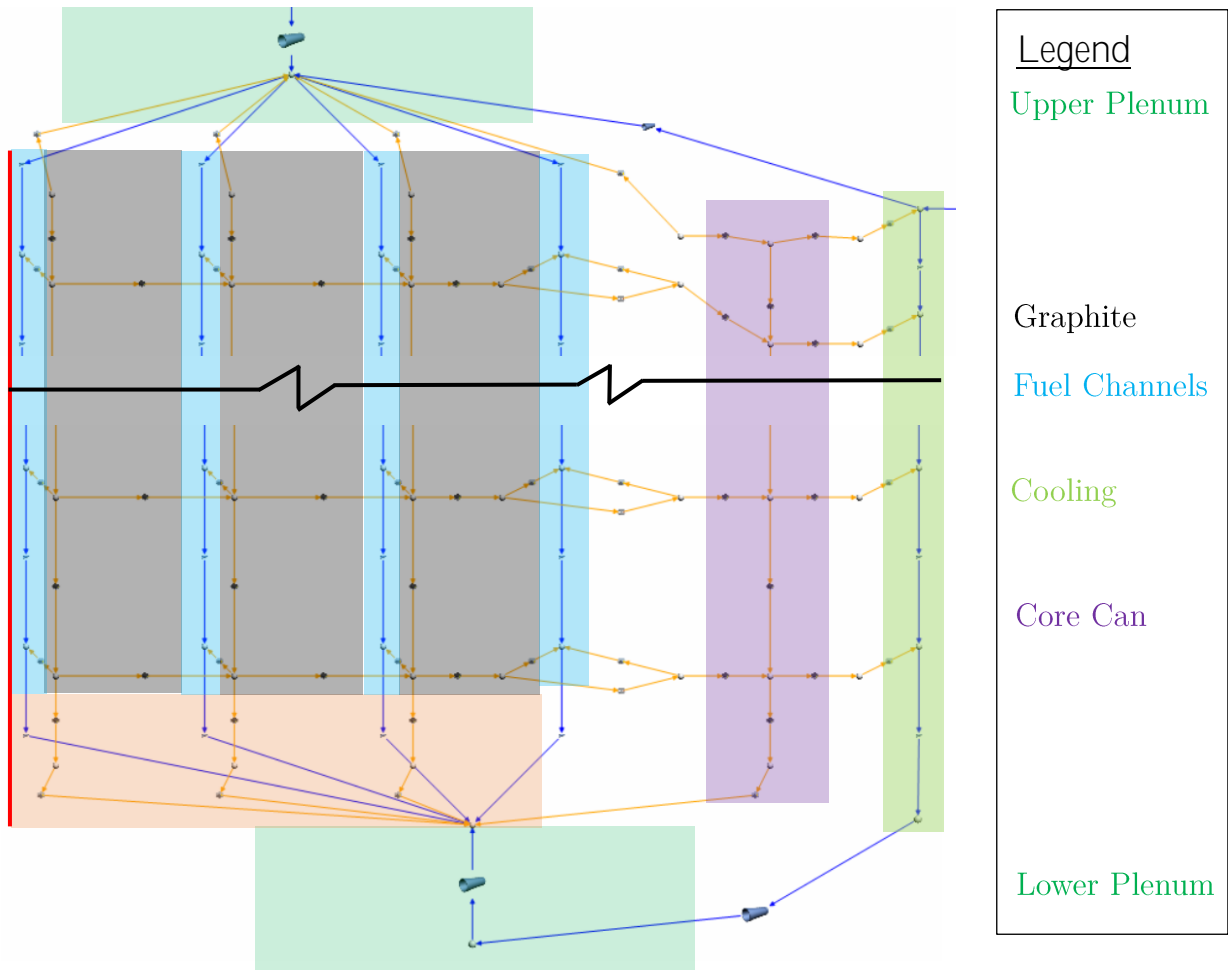


Figure 28: Zoomed Geometry of Flownex Network

Figure 28 shows how the Flownex network is constructed by the Reactor Geometry Chart. The blue arrows represent the fluid flow paths, while the orange arrows represent heat transfer elements. The white circles are node elements; in the fluid flow path, nodes only set the elevation of the layer and heat input in the presence of a power distribution. Between the fluid flow paths, the nodes represent the solid material so have a volume and material specified. Connecting the solid and fluid nodes are convection heat transfer elements; between solid elements are conduction heat transfer elements. As shown in Figure 29, the first three fluid columns represent the core center, bulk, and periphery from left to right. The fourth column is the salt gap – since this region has no solid material for conduction, the element connecting the left and right are for radiation heat transfer.

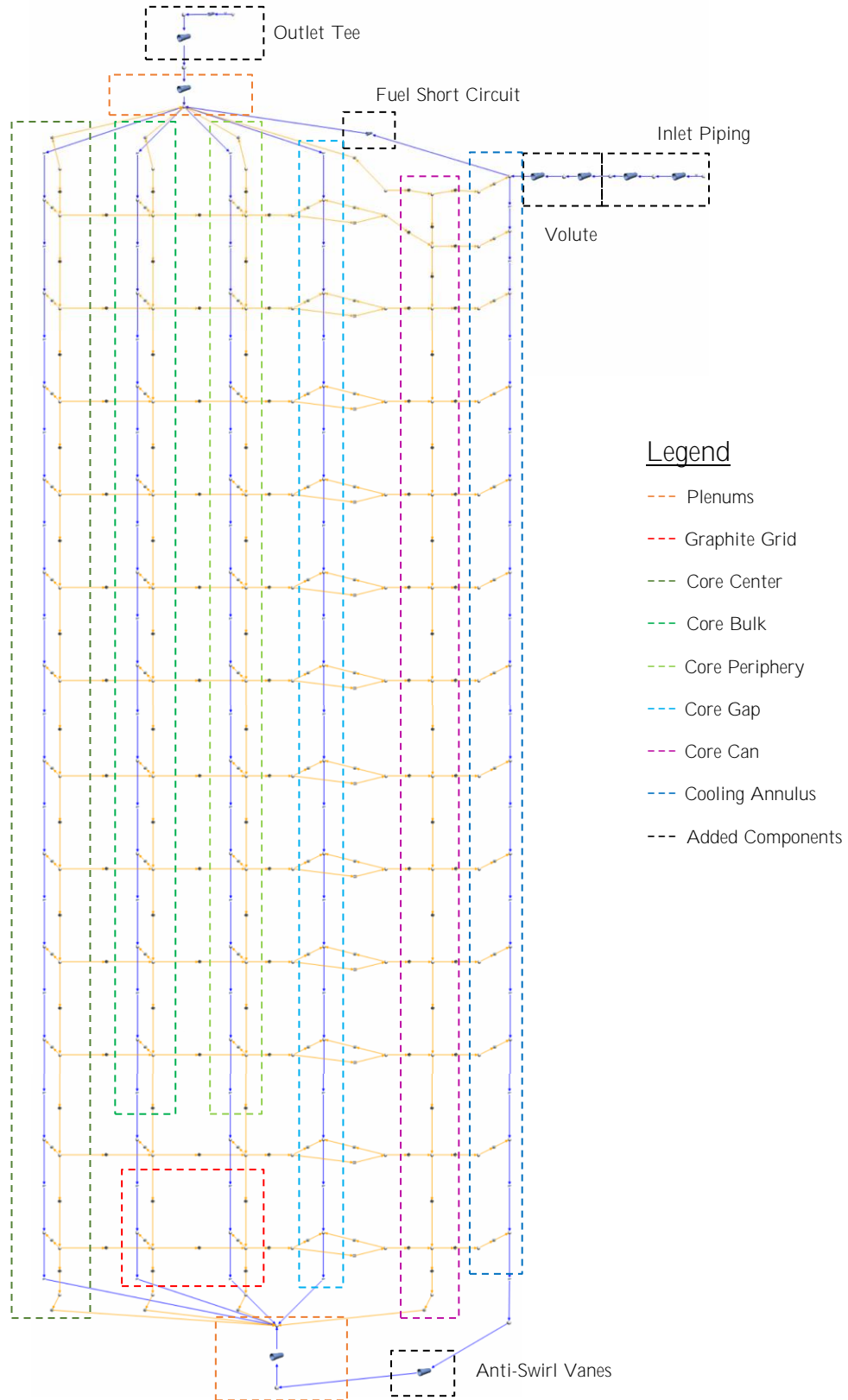


Figure 29: Flownex Network Model of the MSRE Hydraulic Experiment

The length of the cooling annulus components were modified to account for the spiralling flow travelling a much longer length than straight down the annulus. The length was increased to account for the flow going down at an assumed 30° angle. The results of this modification are discussed in Section 5.

4.3.2 Additional Model Components

A few additional model components were added to the network generated from the Reactor Geometry chart.

The 5" inlet pipe and 6" expansion to the distributor were added, with the geometry specified using the built-in pipe schedule database in Flownex. The distributor was added by specifying the circumference and area. The distributor orifices were also added by specifying the total circumference and area of all 84 orifices. The total volume of the vessel inlet through the downcomer was reported as 9.7 ft³; due to the modifications to the downcomer length discussed above, the total volume in the Flownex model of these components is 11.3 ft³ [16].

The anti-swirl vanes were added as a pipe with a variable area. The inlet and outlet circumference and area of a single vane were specified, and the number of vanes in parallel set to 48.

The lower head was modelled as a pipe element with a diameter the same as the core can inner diameter. While the twenty-region model simplifies the lower head to cylindrical geometry and provides the portion of this region that is fuel vs structural elements like the INOR-8 grid, the volume of this region does not match the lower head volume provided elsewhere in the document [16] [49]. Since no other data on the head geometry was found, the more recent report from Robertson [16] was taken as correct; a pipe radius of 70.5 cm and a length of 18.1 cm matches the provided volume of 10 ft³.

The upper head was modelled in a similar way to the lower head, with less complications as there are limited structures in the volume. A pipe element with a radius of 70.5 cm was used, and a length of 19 cm matches the given volume of 10.5 ft³.

The outlet tee was added as two separate pipe elements. The body of the tee was specified as 10" using the built-in pipe schedule database, with a length of 20" as discussed in Section 4.2.1 Minor Losses. The 5" outlet was similarly specified with the schedule database.

5. Hydraulic Model Results Comparison

5.1. Similar Studies of the MSRE

As the only molten salt reactor to operate to date, the MSRE has been the subject of substantial study. A number of studies have been done in other system-level codes, including RELAP5, SAM, TRACE, GOTHIC and MAC [77] [78] [79] [80] [81] [82]. Of these, only the SAM model from Leandro directly discusses the inputs to the model and compares the hydraulic results to the experimental results from Kedl, though the origin of the calculated parameters such as minor losses could not be verified. The RELAP5 model from Carbajo [77] provides comparative results such as velocity and pressure loss, but none of the model inputs; these results are presented along with the current Flownex model results and experimental results where applicable, though the inputs to the model may have been tuned to match experimental flow results as was done with the GOTHIC model. A number of these codes also coupled to neutronics codes such as SERPENT in TRACE [81] and MCNP4c with MAC [82].

Other models of the MSRE have also been made, such as with CFD [53]. This provides interesting information on the flow patterns in some of the complicated structures within the MSRE, but cannot be directly translated to a 1D system code such as Flownex without further study. A publicly available CAD model called OpenMSR is available from Copenhagen Atomics, which provided a convenient tool for investigating areas of complex geometry [54]. Since a number of the structures within the model could not be verified, this model was not used for any input parameters. Finally, a study was conducted for the Nuclear Energy Agency's International Handbook of Evaluated Reactor Physics Benchmark Experiments (IRPhEP) for the MSRE zero-power critical experiment [50]. While this was extremely useful for obtaining geometry, no mention was made of the hydraulic experiment modifications or experimental results, and was more focused on the neutronics of the system.

The above studies all provide useful information, but no complete hydraulic model with inputs and results for all the components of the system could be found. The majority of studies focus on the system neutronics, tune their input values to match the limited experimental results, or make approximations such as the channels being circular [81] [82]. Such approximations can have large effects on the hydraulics of the system, as discussed in Section 5.3. As such, no directly comparable data was found for 1D system codes, though some of the presented results help identify aspects of 1D codes that prevent accurate modelling for complex flows [80] [77].

A summary of the investigation of hydraulic models used in similar studies is available in Appendix B – Summary of Discrepancies in Previous Work and Reported Values.

5.2. Flownex Model vs Experimental Results

A summary of the results of the Flownex model are presented below in Table 3 - Table 6. Results are compared to experimental data where available. Where a range of values were presented, such as along the length of the distributor, the average value is given along with the range of values in brackets. Errors on reported values were assumed to be half the least significant digit, or the error on the reading from the graph, unless otherwise stated. All data is for 1200 gallons/minute and taken from Kedl [37] unless otherwise specified.

The residence times are provided in Table 3. Residence times are an essential parameter for liquid fuel reactors to accurately calculate delayed neutron precursors within the system, required for any type of transient modelling. While the Flownex value for the distributor is half that provided by Robertson [16, p. 93], this is due to half the total distributor length being used in the Flownex model to allow the use of average velocity values. Additionally, the time difference in the cooling annulus is due to the complex 3-dimensional flow that can’t be accurately modelled in a 1-dimensional code, leading to velocity issues shown below in Table 5. This, coupled with the change to the path length of the cooling annulus to approximate the distance travelled by the spiralling flow, leads to incorrect residence times in the annulus and requires further investigation. The average residence time in the core is also reported by Roberston [16, p. 103]. The value of 9.4 seconds in the same report is listed as the time between the two extreme ends of the graphite; this residence time matches the experimental velocity and maximum effective core length shown in Figure 7.

Table 3: Flownex vs Experimental Results - Residence Time [16, p. 102]

Component	Reported Time, s	Flownex, s
Distributor	1.1	0.57
Cooling Annulus	2.43	3.58
Lower Head	3.8	3.74
Core	7.5 (Average)	7.4
Upper Head	3.9	3.93

Table 4 shows the mass flow rate through the system components. The fuel short circuit was assumed to not be present in the hydraulic experiment, but its input parameters were tuned to match the flow rates. Additionally, the input values for the core-can gap were tuned to match the experimental flow rate due to unclear hydraulic parameters. The center channels of the core were measured in two different ways, as discussed in Section 3.3.4 Core.

Table 4: Flownex vs Experimental Results - Mass Flow

Component	Experiment [37], gallons/minute	Flownex, gallons/minute
5” Inlet	1200	1200
Core Center (per channel)	2.3, 3.6-3.7	2.92
Core Bulk (per channel)	1 (1.3 to 0.7)	0.978
Core Periphery (per channel)	-	0.978
Core-can Gap	38.2	38.2
Fuel Short Circuit*	25-50	25

Table 5 lists the velocities, and also compares them with the results from a RELAP5 model [77]. Though the exact input parameters for the RELAP5 model were unknown, the cooling annulus velocity discrepancy exists in both that model and the current Flownex model, indicating a probable modelling challenge for 1D system codes in this region of 3-dimensional flow. The upper plenum also shows significant differences, though the hydraulic experiment only provided values within a few inches of the upper head wall as shown in Figure 19 [37]. CFD results indicate a larger velocity along this streamline than the bulk, with the velocity into the outlet tee

approximately the same as in the Flownex model [53]. The velocity in the lower plenum was provided by Robertson [16]. The velocity for the anti-swirl vanes is the average; due to the expanding cross section, the maximum velocity through the vanes was 0.666 m/s. Finally, the velocity of core center was matched to the value provided by Robertson [16] by varying the inlet minor loss coefficient, due to the large difference in measured flow rates and the unknown inlet geometry at the core center. As can be seen below, the Flownex results match fairly closely to the experimental results, except in regions of complex 3-dimensional flow; this indicates the model will serve as a correct starting point for the residence and transport times when accounting for the delayed neutron precursors in a full MSRE simulation.

Table 5: Flownex vs Experimental Results - Velocity

Component	Experiment [37]		Simulation (m/s)	
	Reported (ft/s)	m/s	Flownex	RELAP5 [77]
5" Inlet	19.2±0.05	5.852±0.015	5.865	5.85
Volute	16.5±0.5 (23-10)	5.03±0.15	4.51	-
Distributor Orifices	11±0.5 (4-18)	3.35±0.15	3.162	-
Cooling Annulus (Top)	11.1±0.05	3.383±0.015	0.655	-
Cooling Annulus (Mid)	7.2±0.05	2.195±0.015		-
Cooling Annulus (Bottom)	5.45±0.05	1.66±0.015		0.66
Anti-Swirl Vanes	-	-	0.377	-
Lower Plenum	0.16±0.005	4.877±0.152x10 ⁻²	4.848 x10 ⁻²	-
Graphite Grid	4.5±0.05	1.372±0.015	1.283	1.25
Core Center*	2.1±0.1	0.64±0.03	0.64	-
Core Bulk/Periphery	0.7±0.05	0.2134±0.015	0.2146	0.23
Upper Plenum	(0.33-0.51)±0.01	(0.1-0.155)±0.003	0.04848	-
Fuel Short Circuit*	-	-	3.40	-
Outlet Tee – 10"	-	-	1.488	-

The pressure loss across components and across the entire assembly is shown in Table 6, with the only reported experimental values obtained from Figure 5 and Figure 14. Results from the RELAP5 model list a pressure loss of 1.78 kPa for the graphite (grid and core) and 44.7 kPa for the system [77]. The results from the SAM model list a loss of 1.91 kPa for the graphite and 44.9 kPa for the system [80]. The large pressure loss through the distributor matches the report by Robertson, listing the distributor as the controlling pressure loss of the system [16, p. 93].

Table 6: Flownex vs Experimental Results - Pressure Loss

Component	Experiment [37]	Flownex, kPa
5" Inlet	-	2.432
6" Volute Inlet	-	0.343
Volute	-	2.479
Distributor Orifices	-	15.786
Cooling Annulus	-	0.259
Anti-Swirl Vanes	-	0.311
Graphite Grid	0.51±0.02 ft-fluid (1.524±0.06 kPa)	1.5374
Core	0.1±0.02 ft-fluid (0.299±0.06 kPa)	0.248
Tee - 10" (inlet)	-	19.282
5" Outlet	-	1.315
Total Loss	15±0.2 ft-fluid (44.8±0.6 kPa)	44.0

5.3. Sensitivity Studies

As previously discussed, there is a substantial amount of conflicting or missing information relating to the exact geometry of the MSRE and hydraulic experiment. Additionally, many of the secondary losses required approximations based on the closest available geometry from experiments or texts. This can have a large impact on the final simulation results, as the complex geometry of the MSRE causes most of the pressure losses [37]. Various simulation model parameters were varied and their impact on the results discussed below. Input values are varied based on known sources of error or geometric tolerances where reported, though for the hydraulic experiment most tolerances are only reported as double those of the MSRE. Where known or assumed values could not be used, values were changed by 10% to determine if the parameter was negligible or not.

5.3.1 Upper Plenum Short Circuit Inclusion

As discussed in Section 3.3.6 Upper Plenum Short Circuit, it was unclear from the available documents whether or not the bypass flow - allowing some portion of fuel salt to flow upwards in the cooling annulus directly into the upper head - was present in the hydraulic experiment. It is also unclear exactly how much flow was diverted this way in the MSRE, as values vary between 25-50 gallons/minute.

While it was assumed that the short circuit was not included in the experiment due to the reported average flow rates through the core seeming to sum to the 1200 gallons/minute flow rate, it is noted that the large uncertainties in the experimentally measured flow rates could account for some of the flow bypassing the core. Figure 17 indicates the flow rate per channel is anywhere between 0.8 and 1.2 gallons per minute in the bulk of the core, with no reported values for the periphery. Additionally, the center 16 channels had a reported flow rate of 2.3-3.7 gallons/minute; the only other available information was that the velocity was approximately 3 times greater than in the core bulk. Thus, the uncertainties in the flow through the core could easily account for the flow required for the bypass while staying in range of the reported values.

A brief sensitivity analysis was undertaken by including the short circuit at 25 gallons/minute of flow. Since the minor loss through the core-can gap was calculated to match the measured experimental value of 38.2 gallons/minute of flow, the value was reduced to $K=102.1$ to match the flow in the gap. No other parameters in the model were changed.

Table 7 shows the change in flow rate and velocity through the core with the inclusion of the fuel short circuit. As can be seen, all the values are well within the experimental uncertainty, though the core bulk channel velocity becomes just outside the experimental value of 0.2134 ± 0.015 m/s.

Table 7: Flow Rate and Velocity for Core including Fuel Short Circuit

Component	Flow rate, gallons/minute		Velocity, m/s	
	No Bypass	With Bypass	No Bypass	With Bypass
Core Center (per channel)	2.92	2.85	0.64	0.625
Core Bulk (per channel)	0.978	0.957	0.2146	0.210
Core-can Gap	38.2	38.2	0.172	
Fuel Short Circuit*	-	25	-	3.39

The pressure loss through the graphite grid was reduced from 1.5374 to 1.473 kPa, and the loss through the core was reduced from 0.248 to 0.235 kPa, though this may be partially attributed to a slight reduction in velocity minorly effecting the minor loss. The rest of the components in the model were negligibly effected, with the total inlet to outlet loss reducing to 43.89 kPa, almost entirely due to the reduced pressure loss through the core. This analysis indicates that the fuel short circuit may have been present in the hydraulic experiment, as the large range in experimental values cannot definitively prove one way or the other.

5.3.2 Graphite Core and Grid

Graphite Grid

The impact of the graphite grid geometry was observed and discussed in depth as a part of the hydraulic experiment studies [37]. As seen in Figure 17, the mass flow rate through the core varies substantially both with radial distance and depending on if the channels sat with the graphite grid directly blocking the entrance.

The loss through the grid is driven by the minor losses. The minor loss and velocity are impacted by the clear flow area through the grid; while the individual orifices are well documented, it is unclear what the total number of orifices are in the grid due to many non-full-size channels at the periphery of the core. The uncertainties in the calculation of the minor loss coefficient, such as from flow area and roughness, can cause a fluctuation of ~0.2 in the minor loss coefficient, which greatly impacts the loss through the grid.

For the grid sensitivity study, the Reactor Geometry Chart was used to re-create the flow network with the new values for the porosity and hydraulic diameter of the graphite grid, using the reported 0.375 ± 0.025 ” for the spacing. It was assumed that the drilled holes were 0.104 ± 0.004 ”. The minor loss was re-calculated as was done for the hydraulic model, using the new flow areas, with new minor losses for the central channels and the core-to-can gap to match experimental values. Table 8 shows the obtained values for the grid; the range represents the variance in the calculated K values as discussed above.

Table 8: Sensitivity Study of the Graphite Grid on Flow Parameters

Parameter	Grid (oversized orifices)	Grid (undersized orifices)
Minor Loss, K	1.531-1.759	1.833-1.587
Velocity, m/s	1.133 (-11.7%)	1.468 (+14.4%)
Pressure Loss, kPa	1.26-1.12 (-18% to -27.2%)	2.22-1.96 (+44.4% to +27.5%)

It is important to note that in the case of the grid with the tolerances added, the velocity through the center channel could not be matched to the reported value of 0.64 m/s, even with a minor loss coefficient of $K=0$, without adjusting the frictional losses in the channels. This could indicate an issue with the frictional loss calculation, which is studied below. However, it seems likely that the grid was undersized instead of oversized, as the velocity with undersized orifices more closely matches the reported velocity value of 1.37 m/s in the grid than the value used in the model. While the values of the minor loss coefficient do not change much with the tolerances, the velocity (and thus the pressure loss) fluctuate substantially.

Core

The graphite core was subject to many investigations to account for the geometry of the fuel channels, as described in Section 4.2. Increasing the total length of the core to 67" - to match the largest reported value – increases the core loss by 0.0055 kPa, or 2.2% of the core loss. This investigation accounted for the additional length being outside the entrance lengths effects on friction factor, and adjusting the central channels and core-can gap inlet losses to match experimental data.

Entrance and exit losses, friction factor, and channel area all impact the losses through the core, with the first 3 being substantially approximated due to the limited experimental data available for the channel geometry. These effects are investigated here; all tests modified the entrance loss of the central core region and the core-to-can gap to maintain a velocity of 0.64 m/s in the central core and a total flow of 38.2 gallons/minute in the gap.

The core inlet loss was modified to $K=1$, which was the lowest found value for a rectangular channel in turbulent flow [64]. This reduces the core loss to 0.218 kPa, a change of -12%. The value was also increased by 20% to $K=2.76$, as the turbulence generated by the graphite grid could not be quantified. This increased the core loss to 0.2586 kPa, a 4.3% increase.

The core outlet loss was reduced to $K=1$, the standard loss to a large volume [56]. The new core loss was 0.243 kPa, a 2.1% reduction.

The used friction factor correction for rectangular channels was about +10% for fully developed flow compared to the values calculated with typical hydraulic diameters [73]. The developing flow entrance length effect was investigated by using a flat friction factor multiplier of 1.1, which reduced the core loss to 0.168 kPa (-32.4%). This was also compared to the value calculated by Flownex using the standard hydraulic diameter, which reduced the core loss to 0.160 kPa (-35.6%).

The friction factor entrance length was approximated heavily as the only available data was for a square channel at a much higher Reynold's number [74]. To determine the impact the friction factor correction had along the entrance length, the calculated friction factor values along the length were varied by $\pm 10\%$ at each element; this led to a change in the pressure loss of $\pm 6.7\%$.

No reported values could be found for the tolerances on the channel dimensions; it was assumed that the tolerances were standard machining tolerances of approximately $\pm 0.005''$ on the channel width and diameter of the rounded ends. This leads to a small variation of 1.6% in the area, 0.55% in the perimeter and 1.1% in the hydraulic diameter of a single channel. Like with the graphite grid, the Flownex network was re-created with the new areas and hydraulic diameters to determine the impact of the tolerances on flow. Unlike the graphite grid, the inlet and outlet minor losses remained the same as there was no dependence on geometry. Increasing the size of the channels resulted in a core pressure loss of 0.2377 kPa (-4.2%), while decreasing the channel size yielded 0.259 kPa (+4.4%). The velocity through the bulk channels was determined to be 0.214 ± 0.003 m/s ($\pm 1.7\%$), while the change in core flow rate per channel was negligible.

The center channel flow was reported as 2.3 or 3.6-3.7 gallons/minute per channel [37]. The velocity is 0.64 ± 0.03 ft/s. Decreasing the center channel flow to 2.3 gallons/minute, the loss through the grid and core became 1.565 and 0.253 kPa respectively. The flow rate per channel in the core bulk also increased to 0.987 gallons/minute and the velocity increased to 0.216 m/s. The highest flow rate that could be obtained in the model by only changing the entrance loss was 3.12 gallons/minute with $K=0$; higher flow rates were only possible by reducing the entrance length friction factor correction. The loss for 3.12 gallons/minute was 1.529 and 0.2464 kPa for the grid and core respectively, and reduced the bulk core flow rate to 0.975 gallons/minute per channel.

A summary of the impact of the variation of the core input parameters on the core pressure loss is presented in Table 9. Clearly the largest impact is due to the entrance effects frictional losses, which require experimental results of the exact geometry to improve the understanding of the effects.

Table 9: Sensitivity Study Results of Core Parameters

Core Varied Value	Effect on Core Loss
Length	+2.2%
Inlet Minor Loss, K	-12% to +4.3%
Outlet Minor Loss, K	-2.1%
No Entrance Length	-32.4%
Entrance Length f corrections	$\pm 6.7\%$
Channel Area	-4.2% to +4.4%
Core Center Flow	+1.8% to 0.6%

5.3.3 Other Model Components

Due to the pressure loss only being provided at a system level (inlet to outlet), it was more challenging to refine the model for the rest of the system. Potential errors were large as many components had unspecified geometric values. Losses presented are specific to the component unless otherwise listed. Components with large individual losses were compared against the effect on the model results to determine their overall impact.

Material Roughness

The material roughness for the carbon steel was varied from 20-100 μm , and aluminum from 15-60 μm as discussed in Section 4.2.3 Hydraulic Model Material Data.

For carbon steel, decreasing the roughness of all components to 20 μm decreased the total pressure loss through the system by 0.73 kPa (-1.7%). Increasing all components to 100 μm increased system loss by 0.35 kPa (+0.8%). This was spread across all inlet and outlet components, with the largest changes being in the pressure loss across individual components such as the 5" outlet (-17.9%), distributor (-9.8%), and distributor inlet (-16%) due to their lengths and velocities. However, the overall system effect is $< 2\%$.

For aluminum, varying the roughness of all components between 15 μm and 60 μm changed the loss through the core and grid by $< \pm 2.5\%$. This was expected as the majority of the loss occurs due to geometry losses and entrance effects.

Roughness would play an increased role in elements with unknown lengths, such as the inlet and outlet pipe. It could also be a factor in the cooling annulus, as the flow path is a spiral and may travel much greater lengths than anticipated.

Inlet

The inlet pipe is a standard 5" schedule 40 pipe; small tolerances are expected on a standard part. Minor losses for reducers are strongly dependent on the area ratio and flow pattern [55]. Changing the area ratio between the 5" inlet and distributor inlet by 1% greatly impacts the minor loss calculation, leading to a $\pm 3.1\%$ change in pressure loss.

The length of the 5" inlet is unknown, with the total pressure loss reported by Kedl [37] as "from the 5-inch inlet pipe to 5-inch outlet pipe". From Figure 4, it appears the pressure sensor is approximately 12" from the 6" volute inlet. Varying the length by 20% results in a $\pm 5.9\%$ change in loss for the component; this piping would be a source of significant pressure loss in the MSRE.

Distributor

The 6" distributor inlet has an unknown length, and was estimated to be 14.8" long from MSRE images. Due to this, the error on this is large; varying the length by 20% produces a $\pm 20\%$ change in pressure loss. However, the loss in this component is small as the minor losses associated with the entrance and exit are calculated in the distributor and 5" inlet, so the impact on the overall pressure loss is small ($< \pm 0.2\%$)

The distributor area was provided, without any information on manufacturing tolerances. Assuming the area provided was $26 \pm 0.1 \text{ in}^2$, the pressure loss is only affected by about 1%. The velocity also changes by a negligible quantity. The distributor was assumed to be perfectly semi-circular; changing the input circumference by 5% effects the pressure loss by 3.8%. The length of the distributor was calculated, and half the length used in the model to represent the average distance travelled by the fluid. The error on the total length is small, as it is associated with the error on the outer diameter of the reactor vessel. A 5% change in average length results in a 3.2% change in pressure loss. Unlike the pipe expansion, a 1% change in the area ratio produces a change in pressure loss of $< 0.5\%$.

The orifices had a well documented but unique geometry. The loss calculation was approximated to orifice stacks in passing flow, neglecting the thickness of the orifices and the inlet angle. Additionally, the velocity along the distributor and through the orifices varied substantially along the length of the distributor. At the inlet of the distributor, the centerline velocity of the distributor and through the orifices were 7 m/s and 1.22 m/s respectively, yielding a minor loss value of $K=6.46$ [55]. At the tail of the distributor, the velocity of the distributor was 3.05 m/s and 5.49 m/s through the orifices, resulting in $K \approx 2.75$. The change in pressure loss through the orifices in the Flownex model was substantial, increasing to 32.4 kPa (+105.2%) if using inlet values or decreasing to 13.9 kPa (-11.9%) if using outlet values instead of the average velocities. While the velocity through the distributor is uniform, as shown in Figure 9, the velocity through the orifices is only listed at the distributor entrance and tail; the orifices stacks are placed more closely together at the inlet and gradually become further spaced along the length [37].

Additionally, the loss could be much lower due to the 30° angle on the orifices. Additional modelling by CFD or experiment is needed to better model the orifices in a 1-D code.

Cooling Annulus

The cooling annulus is the source of the largest discrepancy in the model for the velocity. Since Flownex does not account for gravity other than for total pressure loss due to elevation, no change in inputs to the pipe lengths or elevations effects the velocity or pressure loss excluding elevation. Since the flow path is a spiral, the length of the flow path drives the loss in the section; the losses double if the flow path length doubles. Additionally, the velocity calculated by Flownex is substantially lower than the velocity reported in [37]. This will also greatly affect the losses. In the current model, the losses in the downcomer account for <1% of the total model losses, meaning that increasing the path length has little effect. Since there is no way for Flownex to account for the velocity, which would have a large influence on the loss, further study and an improved model through CFD or experimental analysis is required.

Anti-Swirl Vanes

The anti-swirl vanes are complex in that their exact geometry is not known, and in the MSRE and hydraulic experiment they are actually channels that allow flow out the top which cannot be easily modelled in 1D codes. The vanes change cross section in multiple dimensions along their length due to the bend at the outlet of the cooling annulus. The inlet and outlet circumference and area were varied by 20%; since the minor loss is calculated based on inlet dimensions, the change in inlet area effected the loss by 30%, while the rest of the parameters produced a negligible effect. Increasing the outlet area changed the average velocity by 12%.

The minor loss coefficient was subject to substantial sources of error, with the loss due to a curved diffuser alone being $\pm 20\%$ [58]. The whole minor loss coefficient was varied by 20%, which produced a 20% deviation in the pressure loss. Due to the small pressure loss through the vanes, the overall effect on the system was negligible in all cases. The losses may be larger due to the attenuation of the swirl from the cooling annulus.

Outlet Tee

The outlet tee had a specific geometry due to the large diameter, capped through-run, and reduction through the branch. Values are reported for tees as elbows ($K=1$) [83] or tees with 100% of the flow through the branch ($K=1.1$) [84], though it was shown that exact losses depend on the size of the piping [68]. Additional difficulty stems from many of the reported values not indicating if the velocity of the body of the tee or the branch of the tee were used. Miller [57] provides $K=16.72$ (after velocity scaling) if the tee is filleted. The value was varied by 5% to account for the fillet and other input parameters, effecting the loss by 5.2%. Since this component account for almost half the loss in the system, even this small deviation effects the total system pressure loss by 2.4%.

The length of the 10" pipe was reduced to 10" to match the value reported for the MSRE [16]. Since the loss is dominated by the minor losses from the reducing blanked-off tee, even this 50% change to the length had a negligible effect on the components pressure loss.

The 5” outlet that makes up the branch of the tee has no minor loss associated with it, as it is combined with the tee loss assigned in the 10” pipe component. Similar to the 5” inlet, it was unspecified where the pressure was measured along the outlet pipe. The length of the outlet pipe was varied by 10%, leading to a 10% change in pressure loss in the component. This uncertainty could have a significant impact on the loss in the model, as the outlet length could be much longer in the hydraulic experiment and would have been a long piping run in the MSRE itself.

5.3.4 Summary

A summary of the sensitivity studies and their impact on the pressure loss is presented below in Table 10. Unless otherwise specified, the loss change is at the component level. The largest impact to the model by a wide margin was the orifice minor loss, followed by the outlet tee minor loss. This is expected as these two components accounted for the majority of the loss through the system. Two additional components could substantially affect the system: first, the velocity and path length in the cooling annulus would affect the major loss; and second, the inlet and outlet pipe lengths could have a significant impact on the total pressure loss depending on the length.

Table 10: Summary of Sensitivity Studies of Model Inputs

Component	Parameter	Variation	Effect on ΔP
All	Roughness	20-100 μm (steel) 15-60 μm (aluminum)	Model: -1.7% to +0.8% Components: 0 to -17%
Inlet	Minor Loss	1%	$\pm 3.1\%$
	Length	20%	$\pm 5.9\%$
6” Distributor Inlet	Length	20%	Model: $\pm 0.2\%$ Component: $\pm 20\%$
Distributor	Circumference	5%	$\pm 3.8\%$
	Area	± 0.1 in (0.4%)	$< \pm 1\%$
	Average Length	5%	$\pm 3.2\%$
Orifices	Minor Loss	2.75-6.46	-11.9% to 105.2%
Cooling Annulus	Length	50%	Model: $< \pm 1\%$ Component: $\pm 50\%$
Anti-Swirl Vanes	Area	20%	Model: $< \pm 0.2\%$ Inlet: $\pm 30\%$ Outlet: $\pm 12\%$
	Minor Loss	20%	Model: $< \pm 0.2\%$ Component: $\pm 20\%$
Outlet Tee	Minor Loss	5%	Model: $\pm 2.4\%$ Component: $\pm 5.2\%$
	10” Length	50%	$< 0.1\%$
	5” Length	10%	$\pm 10\%$

6. Conclusions

While there is a substantial amount of missing or conflicting information regarding the Molten Salt Reactor Experiment, it is nevertheless an essential source of experimental data for MSR development. The careful consideration of the available documents, as well as the timeline in which the documents were created, has allowed the creation of a comprehensive hydraulic model of the equivalent hydraulic experiment of the MSRE which was used to obtain the majority of the experimental results available. This has produced input data that may be used as a starting point to create computer simulations of the MSRE that provide accurate velocities and residence times, allowing future computer simulations to accurately model MSRE transients.

Flownex Simulation Environment is a 1-dimensional system level code that contains a number of tools which are beneficial for the modelling and simulation of reactor designs. Features such as integrated C# scripting, neutronics scripts for point kinetics calculations, dedicated nuclear components, and the ability to create custom materials and fluids make it a desirable choice for next generation reactor technologies such as molten salt reactors. The Reactor Geometry Chart component can be used to quickly build flow networks of axisymmetric reactors, allowing for the rapid creation of flow networks and testing of multiple designs.

Flownex was used to create a flow network of the hydraulic experiment of the MSRE, and results were compared against the experimental results. Inputs for the minor pressure losses through the system were calculated from accepted literature values of matching geometry, except in a few instances where the geometry was so complex that no analog was available. Additional corrections were made to the major losses through the core to account for the geometry that could not be modelled exactly in Flownex. These modifications included accounting for the entrance length and geometry of the channels, though large uncertainties were still present due to approximations needed in modelling the irregular geometry of the MSRE system.

The main conclusions from this body of work and the assembled flow network of the hydraulic experiment include the following:

1. A large portion of the MSRE core is in developing flow due to the decay of induced turbulence at the entrance, which must be accounted for manually as Flownex assumes fully developed flow everywhere in the system. This has a significant effect on the hydrodynamics and heat transfer within the core.
2. Attempting to account for developing flow through the core channels requires approximating the entrance length effects. The best approximation for the entrance length leads to a 32% increase in the core loss. This is both non-negligible and a significant approximation, indicating that the true impact could be even greater.
3. The shape of the channels through the graphite core are neither rectangular nor oval, and no exact matching geometry was found in literature. The lack of sharp corners likely reduces the loss compared to a rectangular channel; additionally, it is likely that the heat transfer will be underestimated if using a low aspect ratio rectangular channel as the approximation [69].
4. The largest sources of uncertainty for the system is from the volute orifices and cooling annulus. The orifices occur in irregularly spaced stacks of 3 and are at an angle to the flow – as this could not be calculated from available reference geometries, it is likely that the orifice

losses are overestimated in the Flownex model. However, the true path length of the cooling annulus is unknown, and both Flownex - and all models using 1-dimensional codes found in literature - underestimate the velocity substantially. Thus, the cooling annulus losses are likely higher than calculated in Flownex.

5. The largest pressure losses in the system are through the volute orifices and the outlet reducing tee. Together, they account for almost 80% of the total system pressure loss. Outside of the core, no pressure losses for individual components were obtained in the hydraulic experiment or reported for models found in literature.
6. Many regions of the MSRE exhibit complex 3-dimensional flow patterns that cannot be accounted for in 1-dimensional codes. While this is likely sufficient at a system level, care must be taken for regional effects. Impacted parameters could include values such as fuel residence times.
7. Results for the model may be quite different for other fluids due to differing material properties, such as molten salts. While a thickening agent was added to the water in the hydraulic experiment for some tests to replicate the Reynold's number of molten salt, other properties were not accounted for. For example, molten salts have considerably different Prandtl number, effecting heat transfer.

Overall, the developed model for the hydraulic experiment based on the geometry and additional losses presents reasonable results when compared with the experimental data and comparable models from literature. This model provides the foundation for creating a simulation network of the MSRE in any application. Flownex provides many useful modelling tools for creating such a 1-D thermalhydraulic network, and offers many additional tools to facilitate the extension of the model to the full MSRE operating with molten salts.

6.1. Recommendations for Future Work

The MSRE represents a significant set of experimental results for molten salts and molten salt reactors. The development of a comprehensive MSRE model would be an excellent asset for both the understanding of molten salt reactor design and for potential verification and validation of new simulation software.

Recommendations for future work primarily falls into 3 categories: experimental studies, which will improve the existing fluid dynamic model; heat transfer studies, which will extend the model to the full MSRE and operation with molten salts; and neutronics coupling, which will allow the model to be used for full transient analyses and replicating experiments done on the MSRE. The final category, verifying geometric data, couples with experimental studies in improving the confidence in the existing model. However, this is acknowledged to be unlikely unless further MSRE documents are released publicly.

The future work recommendations are listed below.

- **Model Improvements.** As many of the minor loss coefficients - as well as the major loss corrections through the core channels - are functions of velocity or Reynold's Number, they should be calculated by a script in Flownex to allow testing at multiple flow rates. This is also essential for future work modelling transient responses of the MSRE.

- **Experimental studies.** As described throughout this document, the MSRE contains complex geometry that has no analogous simple geometry. To create a more accurate geometric model, experiments should be conducted to evaluate the most complex regions – namely, the volute and orifices, and the graphite support grid. Additionally, basic fluid dynamic experiments should be conducted on the core channel geometry to better understand the entrance effects and the developing flow. This includes quantifying the effects of the graphite grid obstructing the entrance to the channels.
- **Perform heat transfer studies.** Also noted throughout this document is the likely impact of the geometry on the heat transfer within the MSRE. Extending this model to operation with molten salts, especially with internal heat generation in the case of liquid fuel, comes with additional uncertainties [32]. A number of heat transfer investigations were elaborated on in the MSRE documentation, which require a full investigation to create a complete MSRE model.
- **Coupling with neutronics data.** Substantially more documentation, calculations, and computer models have been created for the neutronics of the MSRE than the thermalhydraulics. To create a complete MSRE model, neutronics data can be coupled with a thermalhydraulic model of the MSRE, with the built-in point kinetics or by data exchange using Flownex's software integration. This would also allow modelling transient type scenarios, such as dynamic experiments that were conducted on the MSRE [85].
- **Verification of geometric data.** Though perhaps unlikely, the clarification of certain geometry values for the MSRE and hydraulic experiment would greatly improve the accuracy of the model. Certain values could be confirmed with as-built drawings, though even obtaining tolerance information of manufactured components could greatly improve the uncertainties listed in Section 5.3. Information such as the length of the inlet and outlet pipes of the hydraulic experiment would help reduce uncertainties in the total pressure drop.

7. References

- [1] International Energy Agency, "Net Zero by 2050: A Roadmap for the Global Energy Sector," IEA, 2021.
- [2] International Energy Agency, "Nuclear Power and Secure Energy Transitions," IEA, 2022.
- [3] International Atomic Energy Agency, "Nuclear Power Reactors in the World," IAEA, Vienna, 2022.
- [4] J. Serp, "The Molten Salt Reactor (MSR) in Generation IV: Overview and Perspectives," *Progress in Nuclear Energy*, vol. 77, pp. 308-319, 2014.
- [5] J. Poignet and J. Fouletier, "Physico-Chemical Properties of Molten Salts," in *Materials Issues for Generation IV Systems*, Dordrecht, Springer, 2008, pp. 523-536.
- [6] B. Elsheikh, "Safety Assessment of Molten Salt Reactors in Comparison with Light Water Reactors," *Journal of Radiation Research and Applied Sciences*, vol. 6, no. 2, pp. 63-70, 2013.
- [7] D. LeBlanc, "Molten salt reactors: A new beginning for an old idea," *Nuclear Engineering and Design*, vol. 240, no. 6, pp. 1644-1656, 2010.
- [8] R. Hargraves and R. Moir, "Liquid Fluoride Thorium Reactors," *American Scientist*, vol. 98, pp. 304-313, 2010.
- [9] A. Vlasov, "Thorium's Long-Term Potential in Nuclear Energy: New IAEA Analysis," International Atomic Energy Agency, 23 March 2023. [Online]. Available: <https://www.iaea.org/newscenter/news/thorium-long-term-potential-in-nuclear-energy-new-iaea-analysis>. [Accessed 15 October 2023].
- [10] International Atomic Energy Agency, "Safety Aspects of Station Blackout at Nuclear Power Plants," IAEA, Vienna, 1985.
- [11] International Atomic Energy Agency, "NO. NR-T-1.19. Terms for Describing Advanced Nuclear Power Plants," IAEA, Vienna, 2021.
- [12] J. Ricci, "Guide to the Phase Diagrams of the Fluoride Systems," Oak Ridge National Lab., Oak Ridge, 1958.
- [13] B. Vriesama, "Aspects of Molten Fluorides as Heat Transfer Agents for Power Generation," TU Delft, Delft, 1979.
- [14] S. Sharma, A. S. Ivanov and C. J. Margulis, "A Brief Guide to the Structure of High-Temperature Molten Salts," *The Journal of Physical Chemistry B*, vol. 6372, no. 125, p. 6359, 2021.
- [15] B. Leng, H. Huang, P. Shi, X. Ye, S. Wang, L. Chang, X. Li and X. Li, "Tribological behavior of 316H stainless steel in NaNO₃-KNO₃ molten salt at Elevated Temperature," *Solar Energy Materials and Solar Cells*, vol. 257, 2023.
- [16] R. Robertson, "ORNL-TM-728. MSRE Design and Operations Report Part I: Description of Reactor Design," Oak Ridge National Laboratory, Oak Ridge, 1965.
- [17] World Nuclear Association, "Molten Salt Reactors," World Nuclear Association, May 2021. [Online]. Available: <https://world-nuclear.org/information-library/current-and-future-generation/molten-salt-reactors.aspx>. [Accessed 15 October 2023].
- [18] W. Yu-ting, L. Bin, M. Chong-fang and G. Hang, "Convective heat transfer in the laminar-turbulent transition region with molten salt in a circular tube," *Experimental Thermal and Fluid Science*, vol. 33, no. 7, pp. 1128-1132, 2009.
- [19] Y. Qiu, M.-J. Li, M.-J. Li, H.-H. Zhang and B. Ning, "Numerical and experimental study on heat transfer and flow features of representative molten salts for energy applications in turbulent tube flow," *International Journal of Heat and Mass Transfer*, vol. 135, pp. 732-745, 2019.

- [20] Z. Ying, B. He, L. Su, Y. Kuang, D. He and C. Lin, "Convective heat transfer of molten salt-based nanofluid in a receiver tube with non-uniform heat flux," *Applied Thermal Engineering*, vol. 181, 2020.
- [21] S. Xiangyang, L. Jianfeng, D. Jing and Y. Jianping, "Convective heat transfer of molten salt in circular tube with nonuniform heat flux," *Experimental Thermal and Fluid Science*, vol. 55, pp. 6-11, 2014.
- [22] C. Chen, Y.-T. Wu, S.-T. Wang and C.-F. Ma, "Experimental investigation on enhanced heat transfer in transversally corrugated tube with molten salt," *Experimental Thermal and Fluid Science*, vol. 47, pp. 108-116, 2013.
- [23] X. Dong, Q. Bi and F. Yao, "Experimental investigation on the heat transfer performance of molten salt flowing in an annular tube," *Experimental Thermal and Fluid Science*, vol. 102, pp. 113-122, 2019.
- [24] H. Hoffman, "Fused Salt Heat Transfer Part II: Forced Convection Heat Transfer in Circular Tubes Containing NaF-KF-LiF Eutectic," Oak Ridge National Laboratory, Oak Ridge, 1955.
- [25] H. Hoffman and S. Cohen, "Fused Salt Heat Transfer - Part III: Forced-Convection Heat Transfer in Circular Tubes Containing the Salt Mixture NaNO₂-NaNO₃-KNO₃," Oak Ridge National Laboratory, Oak Ridge, 1960.
- [26] M. Silverman, W. Huntley and H. Robertson, "Heat Transfer Measurements in a Forced Convection Loop with Two Molten-Fluoride Salts: LiF-BeF₂-ThF₂-UF₄ and Eutectic NaBF₄-NaF," Oak Ridge National Laboratory, Oak Ridge, 1976.
- [27] A. Srivastava, A. Vaidya, N. Maheshwari and P. Vijayan, "Heat transfer and pressure drop characteristics of molten fluoride salt in circular pipe," *Applied Thermal Engineering*, vol. 61, no. 2, pp. 198-205, 2013.
- [28] B.-C. Du, Y.-L. He, Y. Qiu, Q. Liang and Y.-P. Zhou, "Investigation on heat transfer characteristics of molten salt in a shell-and-tube heat exchanger," *International Communications in Heat and Mass Transfer*, vol. 96, pp. 61-68, 2018.
- [29] Q.-L. Kong, J. Qian, H.-W. Zhang, Z.-H. Zhu, W.-G. Huang and W.-H. Li, "Experimental study for shell-and-tube molten salt heat exchangers," *Applied Thermal Engineering*, vol. 124, pp. 616-623, 2017.
- [30] S. He, J. Lu, J. Ding, T. Yu and Y. Yuan, "Convective heat transfer of molten salt outside the tube bundle of heat exchanger," *Experimental Thermal and Fluid Science*, vol. 59, pp. 9-14, 2014.
- [31] Y. Chen, J. Tian, Y. Fu, Z. Tang, H. Zhu and N. Wang, "Experimental study of heat transfer enhancement for molten salt with transversely grooved tube heat exchanger in laminar-transition-turbulent regimes," *Applied Thermal Engineering*, vol. 132, pp. 95-101, 2018.
- [32] L. Luzzi, M. Aufiero, A. Cammi and C. Fiorina, "Thermo-Hydrodynamics of Internally Heated Molten Salts for Innovative Nuclear Reactors," in *Hydrodynamics - Theory and Model*, InTechOpen, 2012, pp. 119-142.
- [33] International Atomic Energy Agency, "Technical Reports Series No. 489. Status of Molten Salt Reactor Technology," IAEA, Vienna, 2021.
- [34] International Atomic Energy Agency, *Advances in Small Modular Reactor Technology Developments - A Supplement to: IAEA Advanced Reactors Information System (ARIS)*, Vienna: IAEA, 2020.
- [35] World Nuclear News, "Chinese molten-salt reactor cleared for start up," World Nuclear News, 9 August 2022. [Online]. Available: <https://world-nuclear-news.org/Articles/Chinese-molten-salt-reactor-cleared-for-start-up>. [Accessed 15 October 2023].
- [36] Ministry of Ecology and Environment of the People's Republic of China, "Notice on issuance of operating license for 2MWt liquid fuel thorium-based molten salt experimental reactor [Translated]," 07 June 2023. [Online]. Available: https://www.mee.gov.cn/xxgk/xxgk09/202306/t20230613_1033619.html. [Accessed 15 October 2023].
- [37] R. Kedl, "ORNL-TM-3229. Fluid Dynamic Studies of the Molten-Salt Reactor Experiment (MSRE) Core," Oak Ridge National Laboratory, 1970.

- [38] Oak Ridge National Laboratory, "ORNL-4622. Molten Salt Reactor Program Semiannual Progress Report For Period Ending August 31, 1970," Oak Ridge National Laboratory, Virginia, 1971.
- [39] M. Fisher, "Spotlight on Innovation: Molten Salt Reactors for a Sustainable Clean Energy Transition," IAEA Department of Nuclear Energy, 24 August 2020. [Online]. Available: <https://www.iaea.org/newscenter/news/spotlight-on-innovation-molten-salt-reactors-for-a-sustainable-clean-energy-transition>. [Accessed 15 October 2023].
- [40] R. Guymon, "ORNL-TM-3039. MSRE Systems and Components Performance," Oak Ridge National Laboratory, Oak Ridge, 1973.
- [41] H. McCoy and B. McNabb, "ORNL-TM-4174. Postirradiation Examination of Materials from the MSRE," Oak Ridge National Laboratory, Oak Ridge, 1972.
- [42] Oak Ridge National Laboratory, "ORNL-3708. Molten-Salt Reactor Program Semiannual Progress Report for Period Ending July 31, 1964," Oak Ridge National Laboratory, Oak Ridge, 1964.
- [43] J. Powers, "First-ever MSR benchmark published, based on ORNL's past and present research," Oak Ridge National Laboratory, [Online]. Available: <https://www.ornl.gov/molten-salt-reactor/measurements>. [Accessed 15 October 2023].
- [44] D. Holcomb, "Module 9: Operating Experience," 7 November 2017. [Online]. Available: <https://www.nrc.gov/docs/ML1733/ML17331B123.pdf>. [Accessed 15 October 2023].
- [45] J. Engel and P. Haubenreich, "Temperatures in the MSRE Core During Steady-State Operation," Oak Ridge National Laboratory, 1962.
- [46] H. MacPherson, "ORNL-3014. Molten-Salt Reactor Program Quarterly Progress Report for Period Ending July 31, 1960," Oak Ridge National Laboratory, Oak Ridge, 1960.
- [47] Oak Ridge National Laboratory, "ORNL-4676. Molten-Salt Reactor Program Semiannual Progress Report for Period Ending February 28, 1971," Oak Ridge National Laboratory, Oak Ridge, 1971.
- [48] R. Swindeman, "ORNL-2780. The Mechanical Properties of INOR-8," Oak Ridge National Laboratory, Oak Ridge, 1961.
- [49] P. Haubenreich, J. Engel, B. Prince and H. Claiborne, "ORNL-TM-730. MSRE Design and Operations Report Part III - Nuclear Analysis," Oak Ridge National Laboratory, Oak Ridge, 1964.
- [50] D. Shen, M. Fratoni, G. Ilas and J. Powers, "Molten-Salt Reactor Experiment (MSRE) Zero-Power First Critical Experiment with 235U," in *International Handbook of Evaluated Reactor Physics Benchmark Experiments*, Nuclear Energy Agency, 2020.
- [51] Oak Ridge National Laboratory, "ORNL-3626. Molten Salt Reactor Program Semiannual Progress Report For Period Ending January 31, 1964," Oak Ridge National Laboratory, Oak Ridge, 1964.
- [52] Flownex Simulation Environment, "Software History," Flownex Simulation Environment, [Online]. Available: <https://flownex.com/about/history/>. [Accessed 15 October 2023].
- [53] K. Podila, Q. Chen and Y. Rao, "CFD Simulations of Molten Salt Reactor Experiment Core," *Nuclear Science and Engineering*, vol. 193, no. 12, pp. 1379-1393, 2019.
- [54] Copenhagen Atomics, "Open MSR - MSRE STEP Files," 17 November 2022. [Online]. Available: https://github.com/openmsr/msre/tree/master/step_files. [Accessed 20 April 2023].
- [55] I. Idelchik, *Handbook of Hydraulic Resistance*, 4th Edition, Redding: begell house, inc., 2007.
- [56] Munson, Okiishi, Huebsch and Rothmayer, *Fundamentals of Fluid Mechanics*, 7th Edition, John Wiley & Sons, Inc., 2013.
- [57] D. Miller, *Internal Flow Systems*, Second Edition, Cranfield: BHRA (Information Services), 1986.

- [58] W. El-Askary, K. Ibrahim, E. Wahba and H. Omara, "Emulsion (Oil-in-Water) Fluid Flow in Curved Diffuser," *International Journal of Fluid Mechanics Research*, vol. 40, no. 3, pp. 204-226, 2013.
- [59] Oak Ridge National Laboratory, "ORNL-3014. Molten-Salt Reactor Program Quarterly Progress Report for Period Ending July 31, 1960," Oak Ridge National Laboratory, Oak Ridge, 1960.
- [60] Flownex Simulation Environment, "General User Manual," Flownex Simulation Environment, 2022.
- [61] B. Gowda, E. Tulapurkara and S. Swain, "Reverse Flow in Channel-Influence of Obstruction Geometry," *Experiments in Fluids*, vol. 16, pp. 137-145, 1993.
- [62] M. Kabir, M. Khan, and M. Bhuiyan, "Flow phenomena in a channel with different shaped obstructions at the entrance," *Fluid Dynamics Research*, vol. 35, no. 6, pp. 391-408, 2004.
- [63] B. Souayeh, S. Bhattacharyya, N. Hdhiri, M. W. Alam, E. Yasin and M. Aamir, "Investigation on inlet obstruction in transitional flow regime: Heat transfer augmentation and pressure drop analysis," *Case Studies in Thermal Engineering*, vol. 34, 2022.
- [64] E. Eckert and T. Irvine Jr., "Incompressible Friction Factor, Transition and Hydrodynamic Entrance Length Studies of Ducts with Triangular and Rectangular Cross-Sections," University of Minnesota, Minneapolis, 1957.
- [65] S. McComas, "Hydrodynamic Entrance Lengths for Ducts of Arbitrary Cross Section," *ASME Journal of Basic Engineering*, vol. 89, no. 4, pp. 847-850, 1967.
- [66] L. Han, "Hydrodynamic Entrance Lengths for Incompressible Laminar Flow in Rectangular Ducts," *Journal of Applied Mechanics*, vol. 27, no. 3, pp. 403-409, 1960.
- [67] A. Kotowski, H. Szewczyk and W. Ciezak, "Entrance Loss Coefficients in Pipe Hydraulic Systems," *Environment Protection Engineering*, vol. 37, no. 4, pp. 105-117, 2011.
- [68] C. Ding, L. Carlson, C. Ellis and O. Mohseni, "Pressure Loss Coefficients of 6, 8 and 10-inch Steel Pipe Fittings," University of Minnesota, Minneapolis, 2005.
- [69] J. Hartnett, J. Koh and S. McComas, "A Comparison of Predicted and Measured Friction Factors for Turbulent Flow Through Rectangular Ducts," *Journal of Heat Transfer*, vol. 84, no. 1, pp. 82-88, 1962.
- [70] L. Hoagland, "Fully developed Turbulent Flow in Straight Rectangular Ducts," Massachusetts Institute of Technology, Boston, 1960.
- [71] H. Duz, "Numerical and Experimental Study to Predict the Entrance Length in Pipe Flows," *Journal of Applied Fluid Mechanics*, vol. 12, no. 1, pp. 155-164, 2019.
- [72] E. Sparrow and A. Chaboki, "Swirl-Affected Turbulent Fluid Flow and Heat Transfer in a Circular Tube," *ASME Journal of Heat and Mass Transfer*, vol. 106, no. 4, pp. 766-773, 1984.
- [73] O. Jones Jr., "An Improvement in the Calculation of Turbulent Friction in Rectangular Ducts," *Journal of Fluids Engineering*, vol. 98, no. 2, pp. 173-180, 1976.
- [74] R. Khan, M. Ali and M. Akhanda, "Study on Friction in Developing Flow Through a Smooth Square Duct," in *4th International Conference on Mechanical Engineering*, Dhaka, 2001.
- [75] Flownex Simulation Environment, "Flownex Library Manual," Flownex Simulation Environment, 2022.
- [76] Flownex Simulation Environment, "Flownex Reactor Model Step-By-Step Example," Flownex Simulation Environment, 2022.

- [77] J. Carbajo, D. De Wet and N. Brown, "Modeling the Molten Salt Reactor Experiment with the RELAP5-3D Code," *Transaction of the American Nuclear Society*, pp. 1503-1505, 11 June 2017.
- [78] C. Shi, Cheng, Maosong and G. Liu, "Development and application of a system analysis code for liquid fueled molten salt reactors based on RELAP5 code," *Nuclear Engineering and Design*, vol. 305, pp. 378-388, 2016.
- [79] J. Lane, R. Harvill, J. Link, S. Claybrook, T. George and T. Kindred, "Steady-State and Transient Benchmarks of GOTHIC to the Molten Salt Reactor Experiment," *Nuclear Technology*, vol. 208, pp. 70-99, 2022.
- [80] A. Leandro, "Modeling the Molten Salt Reactor Experiment with the NEAMS System Analysis Module," The Pennsylvania State University, 2018.
- [81] X. He, "Validation of the TRACE Code for the System Dynamic Simulations of the Molten Salt Reactor Experiment and the Preliminary Study on the Dual Fluid Molten Salt Reactor," Technische Universitat Munchen, Munich, 2016.
- [82] Z. Guo, J. Zhou, D. Zhang, K. S. Chaudri, W. Tian, G. Su and S. Qiu, "Coupled neutronics/thermal-hydraulics for analysis of molten salt reactor," *Nuclear Engineering and Design*, vol. 258, pp. 144-156, 2013.
- [83] Neutrium, "Pressure Loss from Fittings - Excess Head (K) Method," Neutrium, 12 October 2012. [Online]. Available: <https://neutrium.net/fluid-flow/pressure-loss-from-fittings-excess-head-k-method/>. [Accessed 8 July 2023].
- [84] Crane Co., Technical Paper No.410M. Flow of Fluids Through Valves, Fittings and Pipe., The Woodlands: Crane, 1999.
- [85] S. Ball and T. Kerlin, "Experimental Dynamic Analysis of the Molten-Salt Reactor Experiment," Oak Ridge National Laboratory, Oak Ridge, 1966.

Appendix A – Summary of Flownex Model Inputs

A summary of the inputs used in the Flownex model are listed below. A mix of imperial and metric units are used, depending on if the value was obtained from reports or calculated.

Table 11: Complete Flownex Model Inputs

Component	K_{Total}	Input Geometry
5" Inlet	0.1	Length = 12"
Distributor Inlet – 6"	0	L = 14.8"
Distributor	0.089	Circumference = 0.2685 m Area = 26 in ² L = 255.62 cm
Distributor Orifice	3.128	Circumference = 5.02717 m A = 239.42 cm ² Length = 2.54 cm
Anti-Swirl Vanes	1.362 (using minimum area)	Circumference, inlet = 23.729 cm Area, inlet = 23.684 cm C, outlet = 34.734 cm A, outlet = 59.877 cm L = 11" Number in Parallel = 48
Lower Plenum	0	Diameter = 141 cm L = 18.15 cm
Graphite Grid	1.653	See Reactor Chart Inputs Below
Core	See Reactor Chart Inputs Below	
Upper Plenum	0	D = 141 cm L = 19.05 cm
Outlet Tee – 10"	17.42	L = 20"
5" Outlet (tee branch)	0	L = 22"
Fuel Short Circuit	0.186	Circumference = 36.576 cm Area = 4.645 cm ² L = 2.54 cm

Table 12: Complete Reactor Geometry Chart Inputs for the Hydraulic Experiment

Reactor Geometry Chart Zone	K Values	Input Geometry
Graphite Grid	1.653	Height = 5.08 cm D _h = 0.829 cm Core Bulk Permeability = 0.037564 Core Periphery Permeability = 0.022595
Core	Outlet = 1.23	H = 1.589786 m
Core, Central	Inlet = 1.03	D _h = 1.585 cm Perimeter = 0.221655 Radius = 8.128 cm
Core, Bulk	Inlet = 2.3	D _h = 0.0191334 m Permeability = 0.224532 Radius = 58.166 cm
Core, Periphery	Inlet = 2.3	D _h = 1.585 cm P = 0.13505 Radius = 70.1675 cm
Core-Can Gap	Inlet (Core level) = 110.65	Radius = 0.70485 m
Core Can	N/A	Radius = 71.12 cm
Cooling Annulus	-	Radius = 73.66 cm
P = Permeability		

Appendix B – Summary of Discrepancies in Previous Work and Reported Values

This appendix summarizes any discrepancies found in reported values that were required for the creation of a hydraulic model; many of the discrepancies are related to inexact or rounded values being used in reports. These discrepancies include both published reports and available literature that used potentially incorrect values due to missing or conflicting information. More anomalies were observed in the course of this investigation, and this is not intended to be an exhaustive list. This is especially noted for the code-to-code comparisons, depending on the reference (e.g. RELAP, GOthic...), and are not fully presented here.

Table 13: Summary of Major Discrepancies Observed in Key Hydraulic Model Values

Parameter	Description
Core Length	A large variety of reported lengths were found, from 62.125” [16] to 67” in the same document. The variety stems from a number of items, such as the inclusion of the dowels at the end of the stringer, the pyramid shaped top, or just the channel length. Additionally, longer stringers can be seen in images such as Figure 3, though no mention of these were found in reports.
Core Flow Rate	The flow through the core bulk is reported as ‘roughly 1 gallon/minute’ [16]. The two plots of core flow in [16] and [37] are different due to corrections applied to data, and significant scatter in values make it difficult to obtain an accurate average value. Additionally, the 5-region model in [45] show vastly different flow rates for the center region, core periphery, and core-can gap.
Experiment Total Pressure Loss	The system pressure loss as a function of flow rate is substantially larger in the plot by Kedl than the equivalent plot from Robertson [37] [16]. The loss at 1200 gallons/minute is specified as 9.2 ft-fluid by Robertson and about 15 ft-fluid by Kedl, despite having the same slope.
Total Flow Rate	The report by Robertson indicates measurements at 150 and 200 gallons/minute for the total pressure loss, while 300 gallons/minute is the lowest reported by Kedl. The 100% design flow rate is listed as 1225 gallons/minute in Robertson’s distributor velocity distribution plot, though the rest of the document references 1200 gallons/minute.
Flow Measurements	The velocities in the distributor and distributor orifices were slightly different between the Robertson and Kedl reports. Additionally, the velocity at the bottom of the cooling annulus was reported to be 5.5 ft/s by Kedl but only 4.2 ft/s by Robertson.
Core Power	While outside the scope of this research, it was noted that the core power was commonly listed as 10 MW in both ORNL reports and new literature studies [16] [81] (and others). While the reactor was designed for 10 MW, it was run at 7.3 MW [37] [38] [39]. Other reports appear to reference the operating power as 8 MW [77] [79], again due to inexact wording in ORNL reports such as ‘approximately 8 MW’ [40].
Fuel Salt	Initial documents indicate thorium would be used for experiments, but this was later revised to only ²³³ U [16] [40] [41].

The following table is a summary of the hydraulic inputs used in models available in literature.

Below is a brief description of other items of note related to each model. This summary is not a comment on the modelling conducted by the studies, only as an analysis of the different hydraulic parameters used and how they differed from this research. Additionally, the CFD model was left out of the comparison as it is not a 1-D code; however, it was included in the discussion below to understand any simplifications or modifications used.

Table 14: Comparison of Select MSRE Models in Literature

Parameter	RELAP5-3D	RELAP5	GOTHIC	MAC	TRACE	SAM
Correct Fuel Salt	No	-	N	Y	Y	N
Tuned Inputs to Experiment	-	-	Y	-	-	N
Compared to hydraulic experiment	Yes	-	Y	-	N	Y
8 MW Power	Y	Y	Y	Y	10 MW	10 MW
‘ - ‘ Indicates this item was not reported in the literature.						

RELAP5-3D [77]: No report of geometric or loss inputs to the hydraulic model. FLiBe was used as the fuel salt. The software cannot model kinetics or delayed neutrons.

GOTHIC [79]: Inputs to the hydraulic model were tuned to match experimental results; neglects the fuel short circuit. Capable of including point kinetics/delayed neutron simulations.

RELAP5 [78]: No information on hydraulic inputs or comparison to the hydraulic experiment. This report mostly focused on the Molten Salt Breeder Reactor (MSBR).

MAC [82]: This model used circularized channels and states it will not effect the thermohydraulic behaviour of the core. It also states the flow is mainly laminar in the channels, which contradicts the results found by Kedl that the graphite grid will always induce substantial turbulence. It appears to not compare to the experimental results at all, as the report by Kedl is only referenced for the channel geometry.

CFD [53]: A number of simplifications were made to the geometry – the distributor orifice stacks were assumed to be uniformly spaced, and the graphite grid was ignored, neglecting a substantial source of turbulence. It is noted that the flow in the core is in a transition regime.

TRACE [81]: This model made no mention of the report by Kedl or the hydraulic experiment. The model ignored the anti-swirl vanes and support grid, though this is unclear if it is the INOR-8 or graphite grid. This report was mostly focused on point kinetics solving.

SAM [80] – This model was closest to this work. Loss coefficients were calculated with Todreas and Kazimi, but no information provided on how this was done; it appears that all losses through the core were combined to a single entrance loss. No description of core velocities, pressure losses through individual components, etc. was reported when compared with the hydraulic experiment.